



Diversity-oriented generation and biological evaluation of new chemical scaffolds bearing a 2,2-dimethyl-2*H*-chromene unit: Discovery of novel potent ANO1 inhibitors

Yohan Seo^{a,1}, Jiwon Choi^{a,1}, Jeong Hwa Lee^{a,1}, Tae Gun Kim^b, So-hyeon Park^c, Gyoonhee Han^{b,d}, Wan Namkung^{a,d,*}, Ikyon Kim^{a,*}

^a College of Pharmacy and Yonsei Institute of Pharmaceutical Sciences, Yonsei University, 85 Songdogwahak-ro, Yeonsu-gu, Incheon 21983, Republic of Korea

^b Department of Biotechnology, College of Life Science and Biotechnology, Yonsei University, Seoul 03722, Republic of Korea

^c Graduate Program of Industrial Pharmaceutical Science, Yonsei University, Incheon 21983, Republic of Korea

^d Interdisciplinary Program of Integrated OMICS for Biomedical Science Graduate School, Yonsei University, Seoul 03722, Republic of Korea

ARTICLE INFO

Keywords:

Diversity-oriented synthesis
2*H*-Chromene
Chemical space
Anoctamin 1 (ANO1)
Anticancer agent
Apoptosis

ABSTRACT

Chemical territory bearing a 2,2-dimethyl-2*H*-chromene motif was expanded by utilizing an *o*-hydroxy aldehyde group of 5-hydroxy-2,2-dimethyl-2*H*-chromene-6-carbaldehyde as a synthetic handle to install distinctive morphology and functionality of each scaffold. Cell based assays and *in silico* docking analysis led us to discover that these new compounds exhibit inhibitory effect on anoctamin1 (ANO1). ANO1 is amplified and highly expressed in various carcinomas including prostate cancer, esophageal cancer, breast cancer, and pancreatic cancer. Biological assays revealed that (*E*)-1-(7,7-dimethyl-7*H*-furo[2,3-*f*]chromen-2-yl)-3-(1*H*-pyrrol-2-yl)prop-2-en-1-one (**3n**, Ani-FCC) is a novel, potent and selective ANO1 inhibitor with an IC₅₀ value of 1.23 μM. **3n** showed 144 times stronger activity on ANO1 inhibition than ANO2 inhibition and did not alter the chloride channel activity of CFTR and the intracellular calcium signaling. Notably, **3n** strongly decreased cell viability of PC-3 and FaDu cells expressing high levels of ANO1 with a decrease in ANO1 protein levels. In addition, **3n** significantly enhanced apoptosis via activation of caspase 3 and cleavage of PARP in PC-3 and FaDu cells. This study shows that a novel ANO1 inhibitor, **3n**, can be a potential candidate for the treatment of cancers over-expressing ANO1, such as prostate cancer and esophageal cancer.

1. Introduction

2*H*-Chromene, also known as 2*H*-benzopyran, is a substructure of many natural products. More specifically, 2,2-dimethyl-2*H*-chromene moiety is embedded in a number of bioactive natural substances (Fig. 1) [1–5]. Thus, this functional motif has been frequently used as a partial structure of the small-molecule medicinal agents in drug development programs [6–10]. For example, Lee and co-workers developed potent antiangiogenic agents through design and synthesis of ring-truncated deguelin derivatives [11].

Although several systematic approaches to 2*H*-chromene-containing chemical libraries have been demonstrated in the literature [12–14], we envisioned that new chemical space [15–18] having this moiety with distinctive substitution patterns could be further generated by using an

o-hydroxy benzaldehyde group of 5-hydroxy-2,2-dimethyl-2*H*-chromene-6-carbaldehyde (**1**) as a synthetic handle to add structural and functional diversification of each scaffold (Scheme 1) [19–23]. As part of our continued research interest on design, synthesis, and biological evaluation of novel chemical space [24–31], here we wish to report efficient construction and preliminary biological investigation of new chemical libraries based on a 2,2-dimethyl-2*H*-chromene motif [32]. Through biological screening, we were able to discover that these new chromene-based chemical scaffolds inhibit ANO1.

ANO1 plays an important role in a wide range of biological processes in various cell types such as epithelial cells, smooth muscle cells, intestinal pacemaker cells and sensory neurons [33–36]. ANO1 is also highly expressed and plays a pivotal role in cancer progression such as proliferation of cancer cells and metastasis in various carcinomas

* Corresponding authors at: College of Pharmacy and Yonsei Institute of Pharmaceutical Sciences, Yonsei University, 85 Songdogwahak-ro, Yeonsu-gu, Incheon 21983, Republic of Korea (W. Namkung and I. Kim).

E-mail addresses: wnamkung@yonsei.ac.kr (W. Namkung), ikyunkim@yonsei.ac.kr (I. Kim).

¹ These authors contributed equally.

<https://doi.org/10.1016/j.bioorg.2020.104000>

Received 19 October 2019; Received in revised form 21 April 2020; Accepted 3 June 2020

Available online 08 June 2020

0045-2068/ © 2020 Elsevier Inc. All rights reserved.

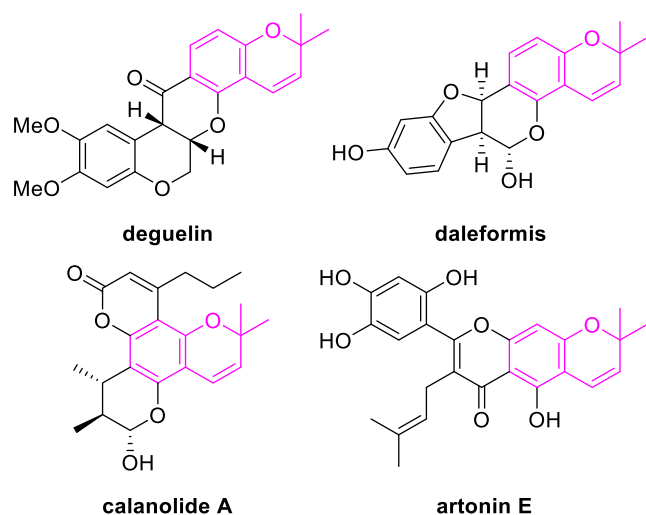


Fig. 1. Some Bioactive Natural Products Having a 2,2-Dimethyl-2H-chromene Unit.

including head and neck squamous cell carcinoma (HNSCC), gastrointestinal, breast, and prostate cancers [37–41]. ANO1 and ANO2 are identified as CaCC (Calcium-activated chloride channel) and share the highest sequence homology between ANO family members (ANO1-ANO10) [42]. ANO2 is highly expressed in olfactory sensory neurons and plays an important role in the regulation of olfactory transduction. Interestingly, recent evidence suggests that ANO2 is involved in the reduction of spike generation in the thalamic cortex and hippocampal CA1 neurons and ANO2 knockout mice show a lack of executive function and severe impairment of motors [43,44].

Previous studies reported that selective downregulation of ANO1 without alteration of ANO2 may provide a novel anticancer therapy [45,46]. ANO1 inhibitors can reduce cell viability by inhibiting calmodulin-dependent protein kinase II (CAMKII) and epidermal growth factor receptor (EGFR) in cancers highly expressing ANO1, such as breast cancer, head and neck cancer, and esophageal squamous cancer (ESCC) [39,47]. ANO1 is overexpressed in prostate cancer and plays pivotal roles in the regulation of chloride efflux and cell volume in androgen-independent prostate cancer [48]. Thus, ANO1 is considered as a potential drug target in various cancers including prostate cancer.

To date, several ANO1 inhibitors have been reported including CaCC_{inh}-A01, tannic acid, T16A_{inh}-A01, idebenone, Ani9, luteolin and Ani9-5f [45,46,49–52]. However, all these inhibitors are in the early stages of drug discovery: novel, potent, and selective ANO1 inhibitors for the drug development are still required. In the present study, novel chemotype ANO1 inhibitors were identified via screening of new chromene-based compounds and their anticancer effects as ANO1 inhibitors were investigated.

2. Results and discussion

2.1. Syntheses of novel 2,2-dimethyl-2H-chromene scaffolds

The starting material **1** was easily prepared in gram quantities by following the known procedure [53,54]. As a means to make a new chemical scaffold from **1**, we first chose the Rap-Stoermer reaction [55,56], which is a condensation reaction of a salicylaldehyde with an α -halocarbonyl compound to give a 2-acylbenzofuran [57–59], a key pharmacophore in many drug discovery researches. Thus, reactions of **1** with several α -bromoketones in the presence of K_2CO_3 were first attempted to synthesize various benzofurans **2** (Scheme 2). The desired 2-acylbenzofurans were obtained in excellent yields.

In addition, an acetyl moiety in **2f** was used for further derivatization: Claisen-Schmidt aldol reactions of **2f** with arylaldehydes provided

chalcones **3** [60] as shown in Scheme 3. Both electron-rich and electron-poor arylaldehydes participated well in these condensations to afford the corresponding enones **3** in good to excellent yields.

The Petasis reaction, also known as the Petasis borono-Mannich reaction, is a three component reaction of an aldehyde, an amine, and a vinyl- or arylboronic acid to form a polyfunctionalized amine [61–63]. Since use of salicylaldehyde as an aldehyde partner of this reaction leads to highly substituted 1,3-amino alcohols [64,65], we applied this reaction to **1** to get benzylamines **4** (Scheme 4). Various 1,3-amino alcohols **4** were readily accessed in good yields under mild conditions. As some biological activities of heterocycles having a 1,3-amino alcohol moiety were known, we hoped that our scaffold **4** may have interesting pharmacological functions.

In addition, reaction of **1** with 4-nitrobenzyl bromide in the presence of KOt-Bu at 160 °C provided the corresponding benzofurans **5a** (Scheme 5) [66,67]. Similarly, benzofuran (**5b**) having a pyridine moiety at C2 position was accessed from **1** and 2-(chloromethyl)pyridine [68].

To evaluate the biological effect of the pyran ring embedded in this series of compounds, compound **7** was synthesized by following the similar procedures as those of **2f** and **3** (Scheme 6).

Biological investigation of the synthesized compounds revealed that the compounds bearing a 2,2-dimethyl-2H-chromene motif such as **3h**, **3n**, **3o**, **3p** and **4d** potentially inhibited ANO1 channel activity with $IC_{50} < 10.2 \mu M$, and **3n** most potently inhibited ANO1 channel activity with an IC_{50} value of 1.23 μM (Table 1). However, compounds having no pyran rings (**7a**, **7b**, and **7c**) did not show an inhibitory effect on ANO1 channel function, indicating the importance of this additional pyran ring on ANO1 inhibition. Based on these observations, further biological study with **3n** was pursued.

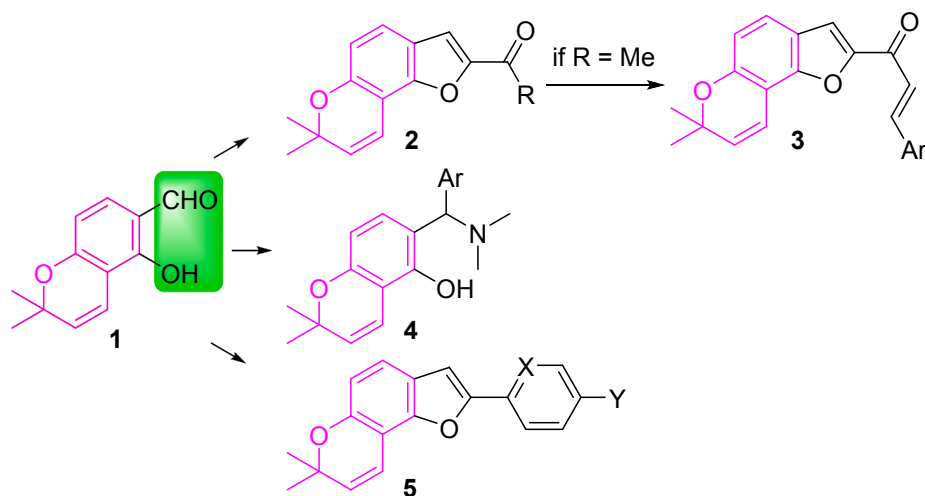
2.2. Inhibitory effect of **3n** on ANO1 channel activity

We further measured the inhibitory effect of **3n** on ANO1, ANO2 and cystic fibrosis transmembrane conductance regulator (CFTR) using YFP fluorescence in FRT cells stably expressing ANO1, ANO2, and CFTR, respectively. As shown in Fig. 2A and 2B, ANO1 and ANO2 calcium-activated chloride channels were activated by ATP, a P2Y receptor agonist. **3n** potently inhibited YFP fluorescence reduction by iodide influx via ANO1, but **3n** weakly inhibited ANO2-mediated YFP fluorescence reduction. **3n** inhibited ANO1 activity ~ 144 times more strongly than ANO2 activity (Fig. 2C). To investigate the effect of **3n** on CFTR channel activity, CFTR was activated by forskolin and inhibited with a specific inhibitor, CFTR_{inh}-172. **3n** did not alter the CFTR-mediated YFP reduction up to 30 μM (Fig. 2D). To observe the effect of **3n** on calcium signaling, the intracellular calcium concentration was increased by ATP in PC-3 cells, and **3n** did not significantly reduce the ATP-induced increase in intracellular calcium concentration up to a concentration of 10 μM indicating complete inhibition of ANO1 (Fig. 2E). These results show that **3n** is an ANO1 inhibitor with higher selectivity for ANO1 compared to ANO2 and CFTR with no effect on intracellular calcium signaling.

2.3. Effect of **3n** on the expression levels of ANO1 protein and cell viability in PC-3 and FaDu cells

Reduction of ANO1 protein is known to significantly inhibit the growth of prostate cancer and hypopharyngeal cancer cells highly expressing ANO1 [69,70]. To investigate the effect of **3n** on the protein expression levels of ANO1, **3n** was treated with different doses in PC-3 and FaDu cells expressing high levels of ANO1. As shown in Fig. 3A and B, **3n** strongly decreased protein expression levels of ANO1 in a dose dependent manner.

To determine whether the reduction of ANO1 protein by **3n** inhibit the proliferation of cancer cells, MTS assay was performed in PC-3 and FaDu cells expressing ANO1 or knockout ANO1. The ANO1 knockout



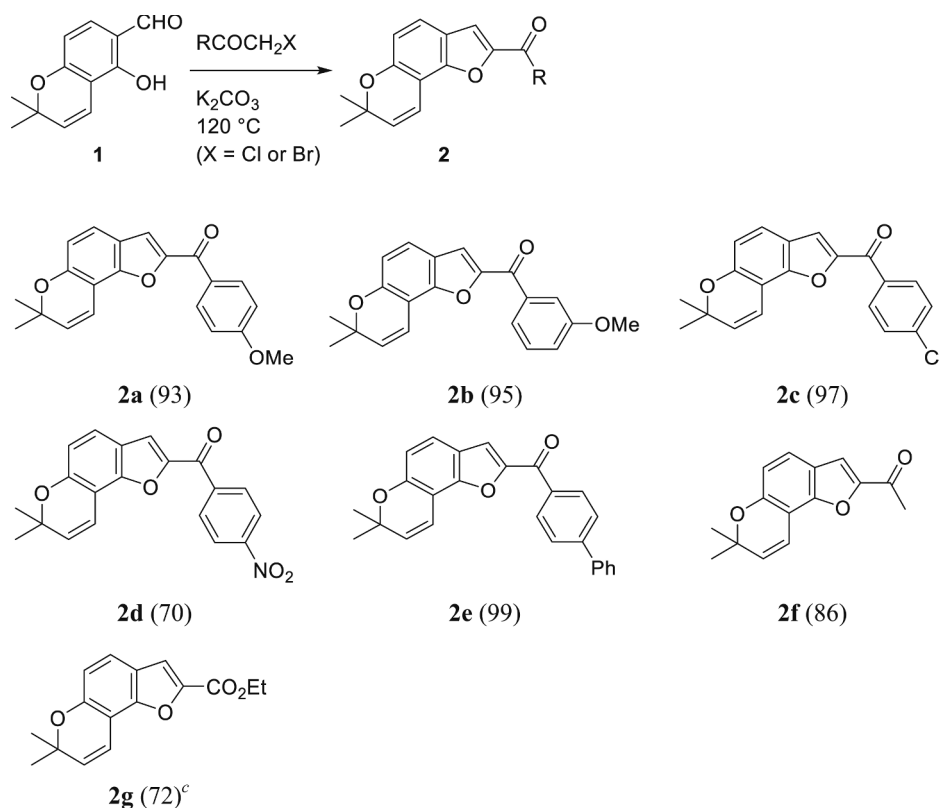
Scheme 1. Synthetic Plans.

cells were established by CRISPR/Cas9 system. While **3n** significantly inhibited cell viability in ANO1 expressing PC-3 and FaDu cells, much less inhibition of cell viability by **3n** in ANO1-knockout PC-3 and FaDu cells was observed (Fig. 3C and 3D). These results suggest that **3n** exhibits anticancer effect via inhibition and reduction of ANO1 protein. Of note, **3n** exhibited ANO1-dependent and ANO1-independent cytotoxicity at high concentrations in PC-3 and FaDu cells (Fig. 3D), indicating that **3n** can also induce apoptosis via ANO1-independent pathways.

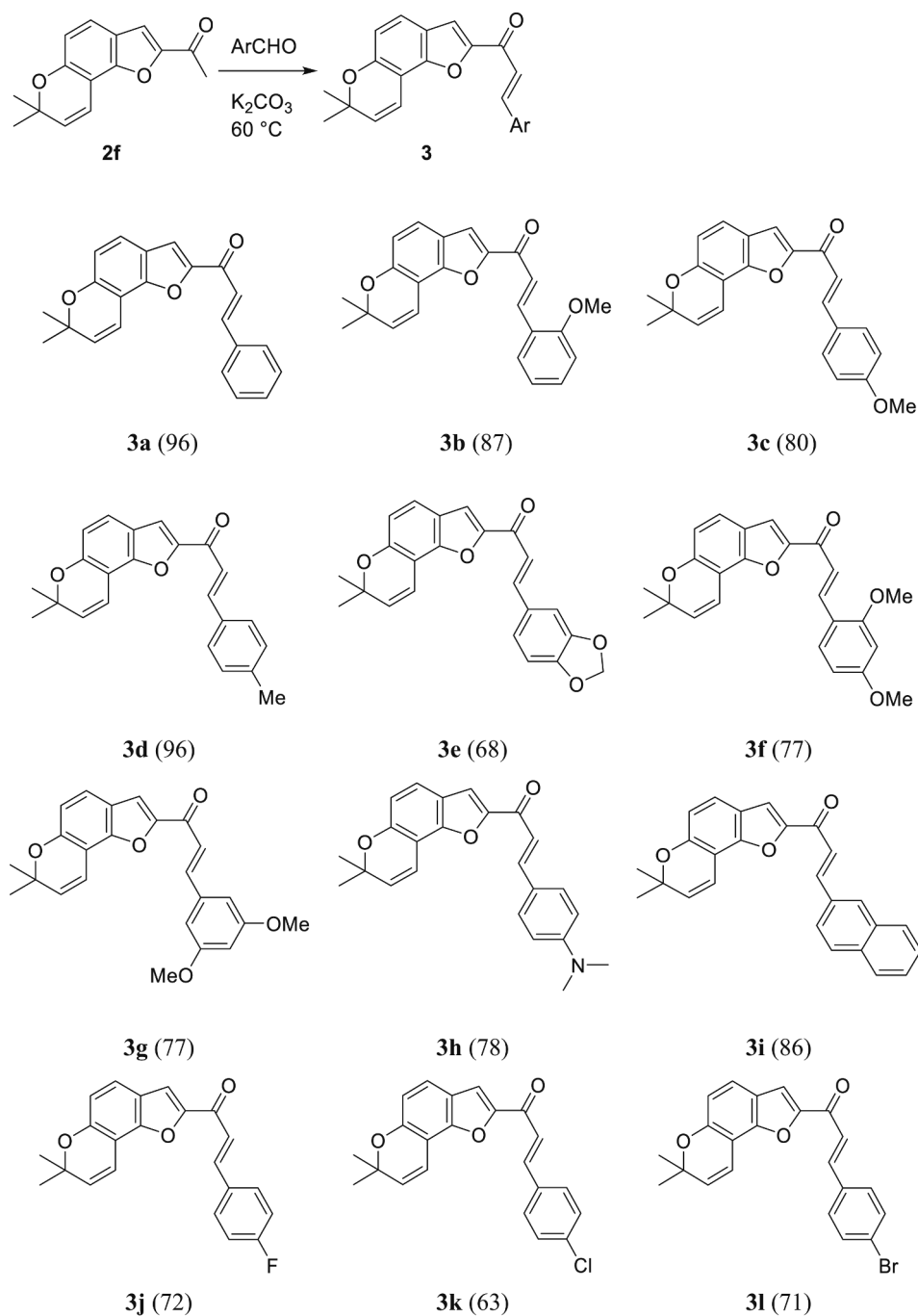
Down regulation of ANO1 significantly induced apoptosis via activation of caspase 3 and cleavage of poly ADP-ribose polymerase (PARP) [71]. To determine whether **3n** exerts its anti-cancer effects via inducing apoptosis in PC-3 and FaDu cells, the effect of **3n** on caspase 3

activity was measured. As shown in Fig. 4A and 4B, the caspase 3 activity was significantly increased by **3n** in a dose dependent manner, but the caspase 3 activation by **3n** was completely blocked by Ac-DEVD-CHO, a potent inhibitor of caspase 3. We stained apoptotic cells with a caspase 3-substrate (NucView® Caspase-3 Substrates), which is cleaved by caspase 3 in apoptotic cells and stains DNA with bright green fluorescence. **3n** significantly increased caspase 3-mediated apoptotic cells in PC3 and FaDu cells (Fig. 4C and 4D). To further investigate the apoptotic mechanism of **3n**, we observed levels of cleaved PARP, a hallmark of apoptosis. The levels of cleaved PARP were significantly increased by **3n** in a dose dependent manner in PC-3 and FaDu cells (Fig. 4E and 4F).

These results revealed that **3n** can induce apoptotic cell death in PC-



Scheme 2. Synthesis of Benzofurans **2^{a-g}**. ^a A mixture of **1** (0.15 mmol), α -haloketone (1.2 equiv), and K_2CO_3 (1.5 equiv) in acetonitrile (2 mL) was stirred at 120 °C. ^b Isolated yield (%). ^c Ethyl bromoacetate (1.2 equiv) was used.



Scheme 3. Synthesis of Chalcones **3**^{a,b}. ^a To a mixture of **2h** (0.12 mmol) and ArCHO (1.2 equiv) in EtOH (1 mL) was added K₂CO₃ (1 equiv) at rt. The reaction mixture was stirred at 60 °C. ^b Isolated yield (%). ^c MeOH was used instead of EtOH.

3 and FaDu cells expressing high levels of ANO1 via inhibition of ANO1 activity and reduction of ANO1 protein levels.

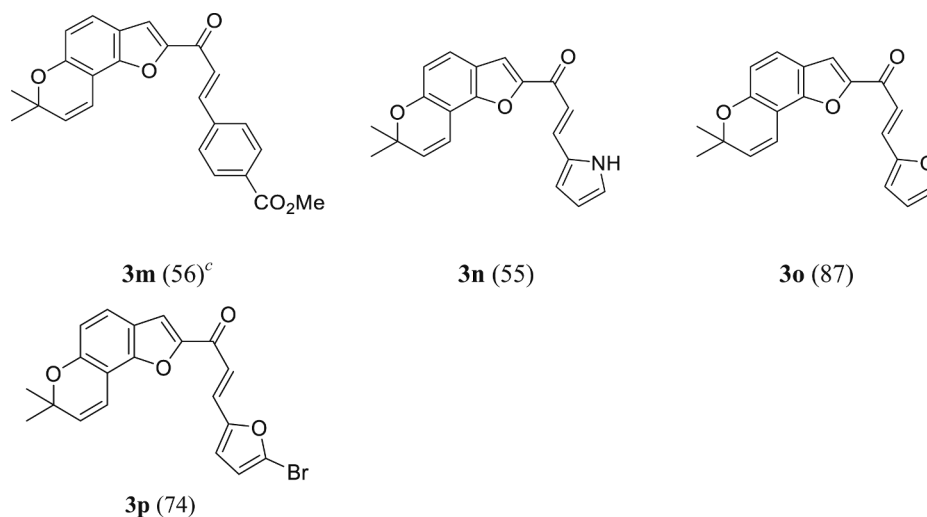
2.4. Molecular docking analysis

A molecular docking study of **3n** to ANO1 was performed using previously reported protein structure and binding sites of ANO1 [72–73]. In Fig. 5A, the binding mode of **3n** was selected by low CDOCKER energy values (-17.22 kcal/mol). As shown in Fig. 5B, **3n** has pi-cation interaction with LYS741, hydrogen bond with LYS645, and

alkyl-hydrophobic interaction with ILE551. The calculated binding energy between **3n** and ANO1 was -51.69 kcal/mol.

3. Conclusions

Several new chemical scaffolds having a 2,2-dimethyl-2H-chromene moiety were established via selective manipulation of the salicylaldehyde group of the starting material and their inhibitory effect of ANO1 was investigated. SAR analysis revealed a novel potent ANO1 inhibitor, **3n** (IC₅₀ = 1.23 μM). Selectivity analysis has shown that **3n** is highly



Scheme 3. (continued)

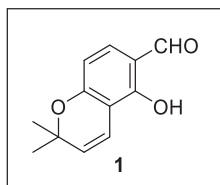
selective for ANO1. **3n** did not alter CFTR activity and calcium signaling, and is 144 times more selective for ANO1 than ANO2. *In vitro* studies showed that **3n** selectively reduced cell viability in an ANO1 dependent manner in PC-3 and FaDu cells. In addition, apoptosis is strongly induced by **3n** via activation of caspase 3 and cleavage of PARP in PC-3 and FaDu cells expressing ANO1. This study could help to identify promising drug candidates for the treatment of cancers with ANO1 upregulation, including prostate cancer and hypopharyngeal cancer.

4. Experimental section

4.1. General methods

Unless specified, all reagents and starting materials were purchased from commercial sources and used as received without purification. "Concentrated" refers to the removal of volatile solvents via distillation using a rotary evaporator. "Dried" refers to pouring onto, or passing through, anhydrous magnesium sulfate followed by filtration. Flash chromatography was performed using silica gel (230–400 mesh) with hexanes, ethyl acetate, and dichloromethane as the eluents. All reactions were monitored by thin-layer chromatography on 0.25 mm silica plates (F-254) visualized with UV light. Melting points were measured using a capillary melting point apparatus. ¹H and ¹³C NMR spectra were recorded on a 400 MHz NMR spectrometer and were described as chemical shifts, multiplicity (s, singlet; d, doublet; t, triplet; q, quartet; m, multiplet), coupling constant in hertz (Hz), and number of protons. HRMS were measured with electrospray ionization (ESI) and Q-TOF mass analyzer.

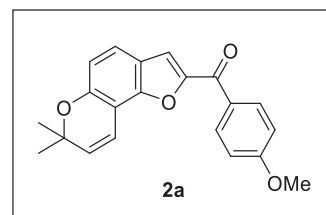
Compound **1** was prepared by following the literature procedure [53,54].



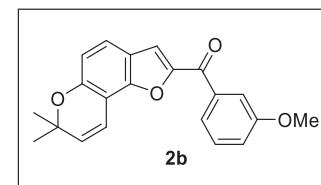
5-Hydroxy-2,2-dimethyl-2H-chromene-6-carbaldehyde (1). Ivory solid, mp: 69.6–70.4 °C; ¹H NMR (400 MHz, CDCl₃) δ 11.65 (s, 1H), 9.66 (s, 1H), 7.29 (d, *J* = 8.4 Hz, 1H), 6.69 (d, *J* = 10.0 Hz, 1H), 6.43 (d, *J* = 8.4 Hz, 1H), 5.61 (d, *J* = 10.0 Hz, 1H), 1.46 (s, 6H); ¹³C NMR (100 MHz, CDCl₃) δ 194.7, 160.7, 158.8, 134.8, 128.7, 115.4, 115.2, 109.6, 109.0, 78.3, 28.6; HRMS (ESI-QTOF) *m/z* [M+H]⁺ calcd for

C₁₂H₁₃O₃ 205.0859, found 205.0864.

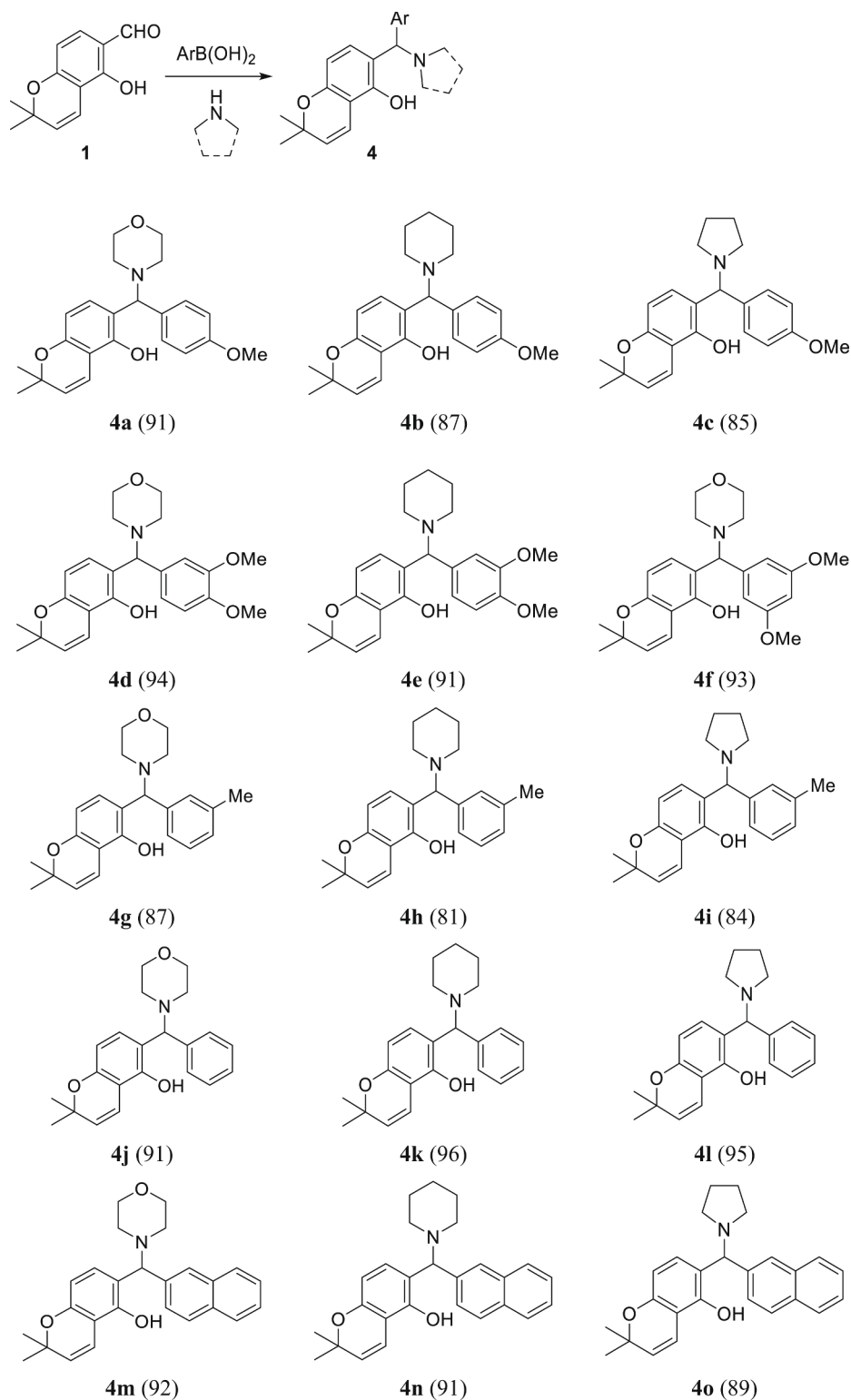
General procedure for the synthesis of 2: To a vial charged with **1** (30 mg, 0.15 mmol) in acetonitrile (2 mL) were added 2-bromo-4'-methoxyacetophenone (40.4 mg, 1.2 equiv) and potassium carbonate (60.9 mg, 3.0 equiv) at room temperature. After being stirred at 120 °C for 4 h, the reaction mixture was concentrated under reduced pressure, extracted with CH₂Cl₂ (2 mL), and washed with H₂O (5 mL). The aqueous layer was extracted with CH₂Cl₂ (1 mL) two more times. The organic layer was dried over MgSO₄, filtered, and concentrated *in vacuo*. The residue was purified by silica gel column chromatography (*n*-hexane:ethyl acetate:dichloromethane = 30:1:2) to give **2a** (45.7 mg, 93%).



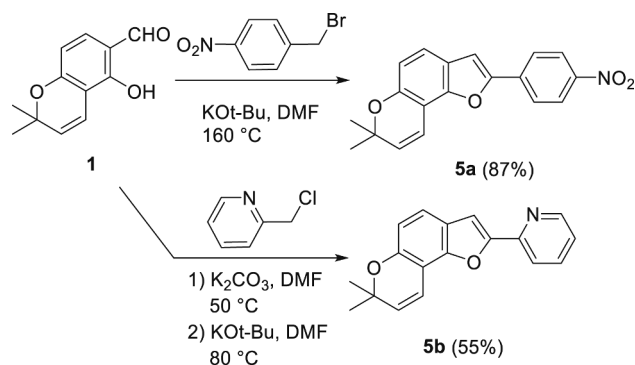
(7,7-Dimethyl-7H-furo[2,3-f]chromen-2-yl)(4-methoxyphenyl)methanone (2a). Brown oil; ¹H NMR (400 MHz, CDCl₃) δ 8.03 (d, *J* = 8.8 Hz, 2H), 7.40–7.37 (m, 2H), 6.97 (d, *J* = 8.8 Hz, 2H), 6.86 (d, *J* = 10.0 Hz, 1H), 6.79 (d, *J* = 8.4 Hz, 1H), 5.69 (d, *J* = 10.0 Hz, 1H), 3.86 (s, 3H), 1.46 (s, 6H); ¹³C NMR (100 MHz, CDCl₃) δ 182.5, 163.4, 153.7, 152.5, 152.5, 131.8, 130.5, 130.3, 122.6, 120.8, 116.8, 115.8, 114.8, 113.9, 106.7, 77.2, 55.6, 28.0; HRMS (ESI-QTOF) *m/z* [M+Na]⁺ calcd for C₂₁H₁₈NaO₄ 357.1097, found 357.1064.



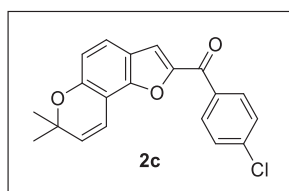
(7,7-Dimethyl-7H-furo[2,3-f]chromen-2-yl)(4-methoxyphenyl)methanone (2b). Yellow solid, mp: 138.9–140.3 °C; ¹H NMR (400 MHz, CDCl₃) δ 7.59 (d, *J* = 7.6 Hz, 1H), 7.50 (s, 1H), 7.44 (s, 1H), 7.42 (s, 1H), 7.40 (s, 1H), 7.15 (dd, *J* = 2.0, 8.4 Hz, 1H), 6.90 (d, *J* = 10.0 Hz, 1H), 6.83 (d, *J* = 8.4 Hz, 1H), 5.72 (d, *J* = 9.6 Hz, 1H), 3.89 (s, 3H), 1.49 (s, 6H); ¹³C NMR (100 MHz, CDCl₃) δ 183.7, 159.8, 154.1, 152.8, 152.0, 139.0, 130.6, 129.6, 122.8, 122.0, 120.7, 119.1, 118.1, 115.8, 115.0, 113.9, 106.7, 77.3, 55.6, 28.0; HRMS (ESI-QTOF) *m/z* [M+Na]⁺ calcd for C₂₁H₁₈NaO₄ 357.1097, found 357.1071.



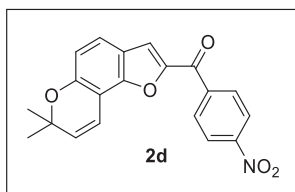
Scheme 4. Synthesis of Benzylamines **4^{a-o}**. ^a A mixture of **1** (0.15 mmol), amine (1.2 equiv), and ArB(OH)_2 (1.2 equiv) in CH_2Cl_2 (1 mL) was stirred at 60 °C for 18 h. ^b Isolated yield (%).



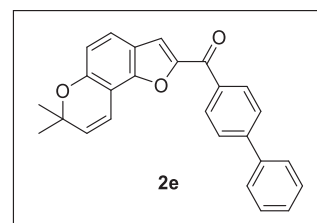
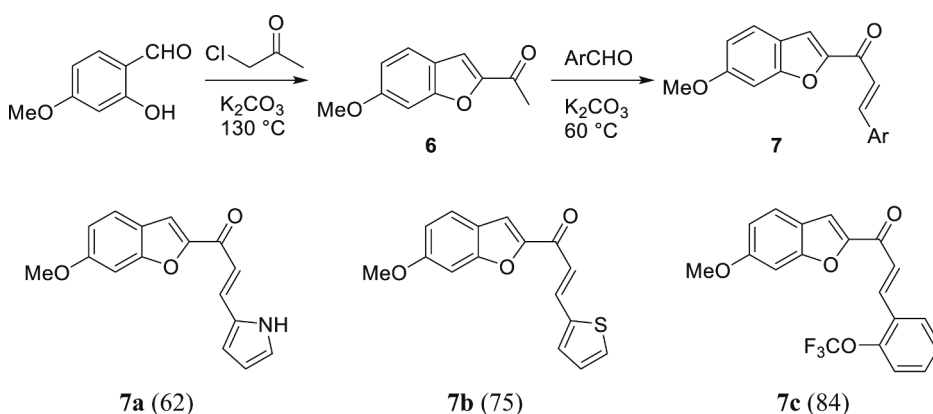
Scheme 5. Synthesis of 5.



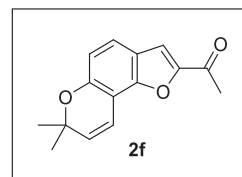
(4-Chlorophenyl)(7,7-dimethyl-7H-furo [2,3-f] chromen-2-yl)methanone (2c). Yellow solid, mp: 88.3–90.8 °C; $^1\text{H NMR}$ (400 MHz, CDCl_3) δ 7.95 (d, $J = 8.4$ Hz, 2H), 7.47 (d, $J = 8.4$ Hz, 2H), 7.42–7.38 (m, 2H), 6.85–6.80 (m, 2H), 5.70 (d, $J = 10.0$ Hz, 1H), 1.47 (s, 6H); $^{13}\text{C NMR}$ (100 MHz, CDCl_3) δ 182.6, 154.2, 151.9, 139.2, 136.0, 130.9, 130.7, 129.0, 125.8, 122.9, 120.7, 117.9, 115.7, 115.2, 106.7, 77.4, 28.0; **HRMS** (ESI-QTOF) m/z $[\text{M}+\text{Na}]^+$ calcd for $\text{C}_{20}\text{H}_{15}\text{ClNaO}_3$ 361.0602, found 361.0655.



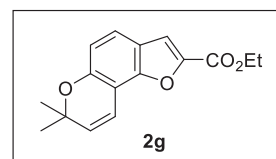
(7,7-Dimethyl-7H-furo [2,3-f] chromen-2-yl)(4-nitrophenyl)methanone (2d). Yellow solid, mp: 140.2–141.0 °C; $^1\text{H NMR}$ (400 MHz, CDCl_3) δ 8.39 (d, $J = 8.8$ Hz, 2H), 8.17 (d, $J = 8.4$ Hz, 2H), 7.50 (s, 1H), 7.45 (d, $J = 8.4$ Hz, 1H), 6.87 (s, 1H), 6.85 (d, $J = 4.4$ Hz, 1H), 5.74 (d, $J = 10.0$ Hz, 1H), 1.50 (s, 6H); $^{13}\text{C NMR}$ (100 MHz, CDCl_3) δ 181.8, 154.7, 153.1, 151.5, 150.1, 142.8, 130.8, 130.4, 123.8, 123.1, 120.6, 118.8, 115.6, 115.4, 106.6, 77.6, 28.1; **HRMS** (ESI-QTOF) m/z $[\text{M}+\text{H}]^+$ calcd for $\text{C}_{20}\text{H}_{16}\text{NO}_5$ 350.1023, found 350.0984.



[1,1'-Biphenyl]-4-yl(7,7-dimethyl-7H-furo [2,3-f] chromen-2-yl)methanone (2e). Ivory solid, mp: 102.9–104.1 °C; $^1\text{H NMR}$ (400 MHz, CDCl_3) δ 8.11 (d, $J = 8.4$ Hz, 2H), 7.75 (d, $J = 8.4$ Hz, 2H), 7.67 (d, $J = 7.2$ Hz, 2H), 7.52–7.48 (m, 3H), 7.44 (d, $J = 8.4$ Hz, 2H), 6.92 (d, $J = 10.0$ Hz, 1H), 6.84 (d, $J = 8.8$ Hz, 1H), 5.73 (d, $J = 10.0$ Hz, 1H), 1.50 (s, 6H); $^{13}\text{C NMR}$ (100 MHz, CDCl_3) δ 183.5, 154.1, 152.8, 152.2, 145.5, 140.1, 136.5, 135.3, 130.6, 130.1, 129.1, 128.4, 127.5, 127.3, 122.8, 120.8, 117.7, 115.8, 115.1, 106.7, 77.4, 28.0; **HRMS** (ESI-QTOF) m/z $[\text{M}+\text{H}]^+$ calcd for $\text{C}_{26}\text{H}_{21}\text{O}_3$ 381.1485, found 381.1441.



1-(7,7-Dimethyl-7H-furo [2,3-f] chromen-2-yl)ethan-1-one (2f). Yellow solid, mp: 107.9–109.8 °C; $^1\text{H NMR}$ (400 MHz, CDCl_3) δ 7.42 (s, 1H), 7.39 (d, $J = 8.4$ Hz, 1H), 6.85 (d, $J = 10.0$ Hz, 1H), 6.81 (d, $J = 8.4$ Hz, 1H), 5.71 (d, $J = 10.0$ Hz, 1H), 2.57 (s, 3H), 1.48 (s, 6H); $^{13}\text{C NMR}$ (100 MHz, CDCl_3) δ 188.0, 153.9, 152.5, 152.4, 130.6, 122.7, 120.7, 115.7, 114.9, 114.3, 106.7, 77.3, 28.0, 26.4; **HRMS** (ESI-QTOF) m/z $[\text{M}+\text{Na}]^+$ calcd for $\text{C}_{15}\text{H}_{14}\text{NaO}_3$ 265.0835, found 265.0796.



Ethyl 7,7-dimethyl-7H-furo [2,3-f] chromene-2-carboxylate (2g). White solid, mp: 54.6–56.8 °C; $^1\text{H NMR}$ (400 MHz, CDCl_3) δ 7.43 (s, 1H), 7.36 (d, $J = 8.8$ Hz, 1H), 6.88 (d, $J = 10.0$ Hz, 1H), 6.80 (d, $J = 8.4$ Hz, 1H), 5.70 (d, $J = 9.6$ Hz, 1H), 4.41 (q, $J = 7.0$ Hz, 2H), 1.47 (s, 6H), 1.41 (t, $J = 7.0$ Hz, 3H); $^{13}\text{C NMR}$ (100 MHz, CDCl_3) δ 159.6, 153.0, 152.1, 145.0, 130.3, 122.0, 120.5, 115.7, 114.4, 106.6, 61.2, 27.8, 14.3; **HRMS** (ESI-QTOF) m/z $[\text{M}+\text{Na}]^+$ calcd for $\text{C}_{16}\text{H}_{16}\text{NaO}_4$ 295.0941, found 295.0968.

General procedure for the synthesis of 3: To a vial charged with **2f** (30 mg, 0.12 mmol) and benzaldehyde (15.2 μl , 1.2 equiv) in ethanol

Scheme 6. Synthesis of **7**^{a,b}. ^a A mixture of 2-hydroxy-4-methoxybenzaldehyde (1.97 mmol), chloroacetone (1.2 equiv), and K_2CO_3 (3.0 equiv) in acetonitrile (6.6 mL) was stirred at 130 °C. To a mixture of **6** (0.16 mmol) and ArCHO (1.2 equiv) in EtOH (1 mL) was added K_2CO_3 (1.0 equiv) at rt. The reaction mixture was stirred at 60 °C. ^b Isolated yield (%).

Table 1
ANO1 inhibition by a 2,2-Dimethyl-2H-chromene derivatives^a.

Compound	Structure	IC ₅₀ (μM) of ANO1
2a		NA ^b
2b		NA
2c		NA
2d		NA
2e		NA
2f		NA
2g		NA
3a		NA
3b		NA
3c		NA
3d		NA

Table 1 (continued)

Compound	Structure	IC ₅₀ (μM) of ANO1
3e		NA
3f		NA
3g		NA
3h		4.33
3i		NA
3j		NA
3k		NA
3l		NA

(continued on next page)

Table 1 (continued)

Compound	Structure	IC ₅₀ (μM) of ANO1
3m		NA
3n		1.23
3o		1.73
3p		10.2
4a		NA
4b		NA
4c		NA
4d		5.26
4e		NA

Table 1 (continued)

Compound	Structure	IC ₅₀ (μM) of ANO1
4f		NA
4g		NA
4h		NA
4i		NA
4j		NA
4k		NA
4l		NA
4m		NA
4n		NA

(continued on next page)

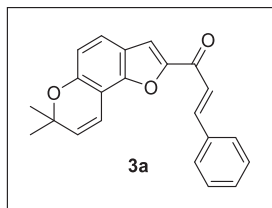
Table 1 (continued)

Compound	Structure	IC ₅₀ (μM) of ANO1
4o		NA
1		NA
5a		NA
5b		NA
7a		NA
7b		NA
7c		NA

^a IC₅₀ values were determined using YFP fluorescence quenching assay in FRT cells expressing ANO1 (mean ± S.E., n = 3).

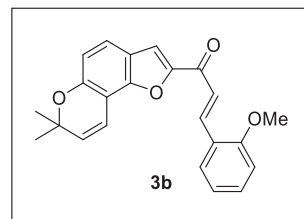
^b NA when the inhibition rate at 100 μM is < 20%.

(1 mL) was added K₂CO₃ (17.1 mg, 1.0 equiv) at room temperature. After being stirred at 60 °C for 3 h, the reaction mixture was concentrated under reduced pressure, extracted with CH₂Cl₂ (2 mL), and washed with H₂O (5 mL). The water layer was extracted with CH₂Cl₂ (1 mL) two more times. The organic layer was dried over MgSO₄, filtered, and concentrated *in vacuo*. The residue was purified by silica gel column chromatography (*n*-hexane:ethyl acetate:dichloromethane = 50:1:2) to give **3a** (38.1 mg, 96%).

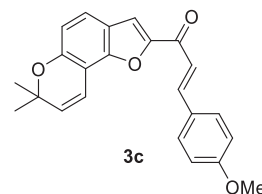


(E)-1-(7,7-Dimethyl-7H-furo [2,3-f] chromen-2-yl)-3-phenylprop-2-en-1-one (3a). Yellow solid, mp: 98.1–99.6 °C; ¹H NMR (400 MHz, CDCl₃) δ 7.92 (d, *J* = 15.6 Hz, 1H), 7.69–7.67 (m, 2H), 7.58 (s, 1H), 7.53 (d, *J* = 15.6 Hz, 1H), 7.44–7.42 (m, 4H), 6.93 (d, *J* = 9.6 Hz, 1H), 6.83 (d, *J* = 8.4 Hz, 1H), 5.73 (d, *J* = 10.0 Hz, 1H), 1.50 (s, 6H); ¹³C

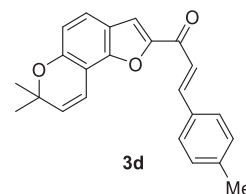
NMR (100 MHz, CDCl₃) δ 179.1, 154.0, 153.6, 152.6, 144.1, 134.9, 130.8, 130.5, 129.1, 128.7, 122.8, 121.5, 121.0, 115.8, 115.0, 114.5, 106.7, 77.3, 28.0; HRMS (ESI-QTOF) *m/z* [M+Na]⁺ calcd for C₂₂H₁₈NaO₃ 353.1148, found 353.1122.



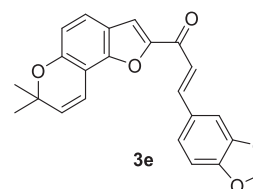
(E)-1-(7,7-Dimethyl-7H-furo [2,3-f] chromen-2-yl)-3-(2-methoxyphenyl)prop-2-en-1-one (3b). Yellow solid, mp: 143.3–144.2 °C; ¹H NMR (400 MHz, CDCl₃) δ 8.24 (d, *J* = 16.0 Hz, 1H), 7.68 (dd, *J* = 1.2, 7.6 Hz, 1H), 7.61 (d, *J* = 15.6 Hz, 1H), 7.55 (s, 1H), 7.43–7.37 (m, 2H), 7.00 (t, *J* = 7.6 Hz, 1H), 6.94 (t, *J* = 10.0 Hz, 2H), 6.82 (d, *J* = 8.4 Hz, 1H), 5.73 (d, *J* = 10.0 Hz, 1H), 3.94 (s, 3H), 1.49 (s, 6H); ¹³C NMR (100 MHz, CDCl₃) δ 179.7, 159.1, 153.9, 153.8, 152.5, 139.6, 132.0, 130.5, 129.4, 123.9, 122.7, 122.2, 121.1, 120.8, 115.9, 114.8, 114.2, 111.4, 106.7, 77.2, 55.7, 28.0; HRMS (ESI-QTOF) *m/z* [M+Na]⁺ calcd for C₂₃H₂₀NaO₄ 383.1254, found 383.1251.



(E)-1-(7,7-Dimethyl-7H-furo [2,3-f] chromen-2-yl)-3-(4-methoxyphenyl)prop-2-en-1-one (3c). Yellow solid, mp: 138.8–139.3 °C; ¹H NMR (400 MHz, CDCl₃) δ 7.89 (d, *J* = 15.6 Hz, 1H), 7.64 (d, *J* = 8.4 Hz, 1H), 7.56 (s, 1H), 7.44 (s, 1H), 7.41 (d, *J* = 5.2 Hz, 1H), 6.94 (t, *J* = 9.6 Hz, 3H), 6.83 (d, *J* = 8.8 Hz, 1H), 5.73 (d, *J* = 9.6 Hz, 1H), 3.87 (s, 3H), 1.49 (s, 6H); ¹³C NMR (100 MHz, CDCl₃) δ 178.1, 160.9, 152.8, 151.5, 142.9, 129.5, 129.5, 126.6, 121.6, 120.0, 118.1, 114.8, 113.8, 113.5, 113.0, 105.7, 102.8, 76.2, 54.5, 27.0; HRMS (ESI-QTOF) *m/z* [M+Na]⁺ calcd for C₂₃H₂₀NaO₄ 383.1254, found 383.1213.



(E)-1-(7,7-Dimethyl-7H-furo [2,3-f] chromen-2-yl)-3-(p-tolyl)prop-2-en-1-one (3d). Yellow solid, mp: 136.4–137.8 °C; ¹H NMR (400 MHz, CDCl₃) δ 7.90 (d, *J* = 15.6 Hz, 1H), 7.59–7.57 (m, 3H), 7.49 (d, *J* = 16.0 Hz, 1H), 7.42 (d, *J* = 8.4 Hz, 1H), 7.23 (d, *J* = 8.0 Hz, 1H), 6.93 (d, *J* = 10.0 Hz, 1H), 6.83 (d, *J* = 8.4 Hz, 1H), 5.73 (d, *J* = 9.6 Hz, 1H), 2.40 (s, 3H), 1.49 (s, 6H); ¹³C NMR (100 MHz, CDCl₃) δ 179.2, 153.9, 153.8, 152.5, 144.2, 141.4, 132.2, 130.5, 129.9, 129.4, 128.8, 127.3, 122.7, 121.0, 120.4, 115.8, 114.9, 114.3, 106.7, 77.3, 28.0, 21.7; HRMS (ESI-QTOF) *m/z* [M+Na]⁺ calcd for C₂₃H₂₀NaO₃ 367.1305, found 367.1350.



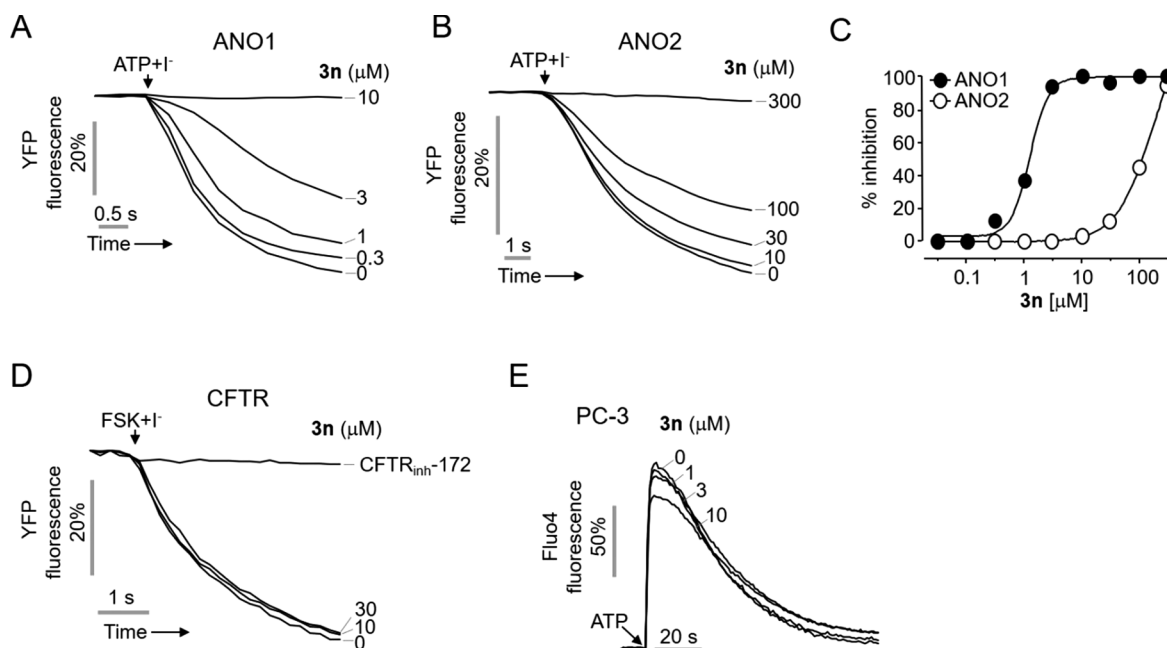


Fig. 2. Identification and characterization of **3n**, a novel ANO1 inhibitor. (A-B) Effect of **3n** on ANO1 and ANO2 activity in FRT-YFP cells expressing ANO1 and ANO2. The cells were pretreated with the indicated concentrations of **3n** for 20 min and then ANO1 and ANO2 was activated by 100 μM ATP. (C) Summary of dose responses (mean ± S.E., n = 3). (D) Effect of **3n** on CFTR activity in FRT-YFP cells expressing human CFTR. CFTR was activated by 10 μM forskolin (FSK) and blocked by 10 μM CFTR_{inh}-172. (E) Intracellular calcium concentration was measured using Fluo4 in PC-3 cells. The cells were pretreated with 1, 3 and 10 μM of **3n** for 20 min, then 100 μM ATP was applied.

(E)-3-(Benzo[d][1,3]dioxol-5-yl)-1-(7,7-dimethyl-7H-furo[2,3-f]chromen-2-yl)prop-2-en-1-one (3e). Yellow solid, mp: 71.6–72.8 °C; ¹H NMR (400 MHz, CDCl₃) δ 7.84 (d, J = 15.6 Hz, 1H), 7.55 (s, 1H), 7.42 (d, J = 8.4 Hz, 1H), 7.37 (d, J = 15.6 Hz, 1H), 7.21 (s, 1H), 7.16 (d, J = 8.0 Hz, 1H), 6.92 (d, J = 10.0 Hz, 1H), 6.86 (d, J = 8.0 Hz,

1H), 6.82 (d, J = 8.4 Hz, 1H), 6.04 (s, 2H), 5.73 (d, J = 10.0 Hz, 1H), 1.49 (s, 6H); ¹³C NMR (100 MHz, CDCl₃) δ 179.1, 153.9, 152.5, 150.2, 148.6, 143.9, 130.5, 129.4, 125.7, 122.7, 121.1, 119.5, 115.8, 114.9, 114.1, 108.9, 106.9, 106.7, 101.8, 77.3, 29.9, 28.0; **HRMS** (ESI-QTOF) m/z [M + H]⁺ calcd for C₂₃H₁₉O₅ 375.1227, found 375.1264.

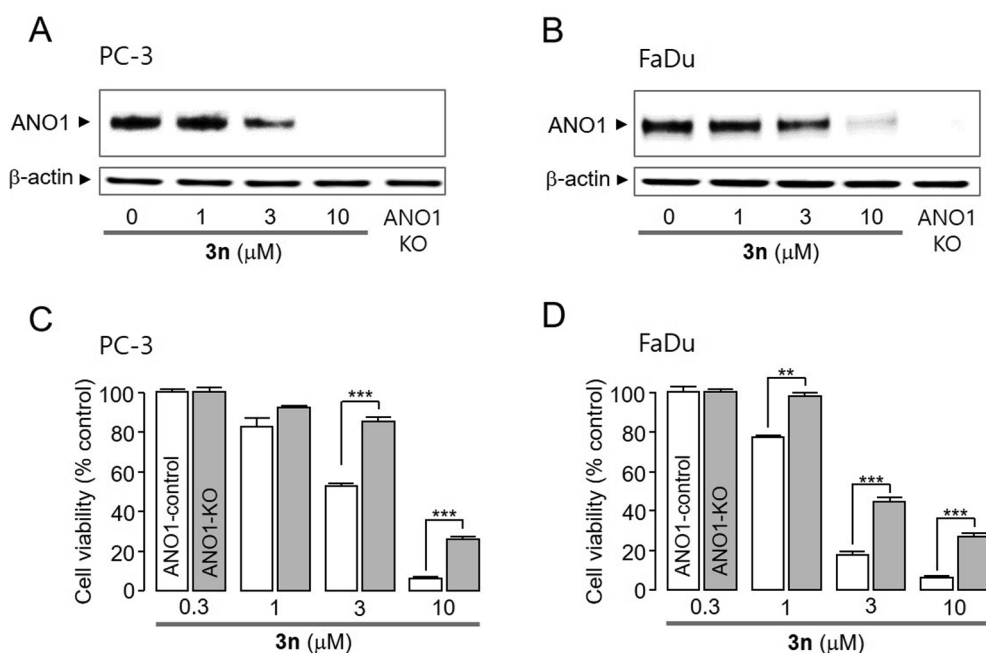


Fig. 3. Effect of **3n** on protein expression levels of ANO1 and cell viability in PC-3 and FaDu cells. (A-B) Western blot analysis of ANO1 in PC-3 and FaDu cells expressing ANO1. Cells were cultured with indicated concentration of **3n** for 24 h. ANO1-knockout (KO) PC-3 or FaDu cells were used as control. (C-D) PC-3 and FaDu cells expressing ANO1 or ANO1-knockout were treated with **3n** at the indicated concentration for 48 h. Cell viability was measured by MTS analysis (mean ± S.E., n = 3). *P < 0.05 **P < 0.01, ***P < 0.001.

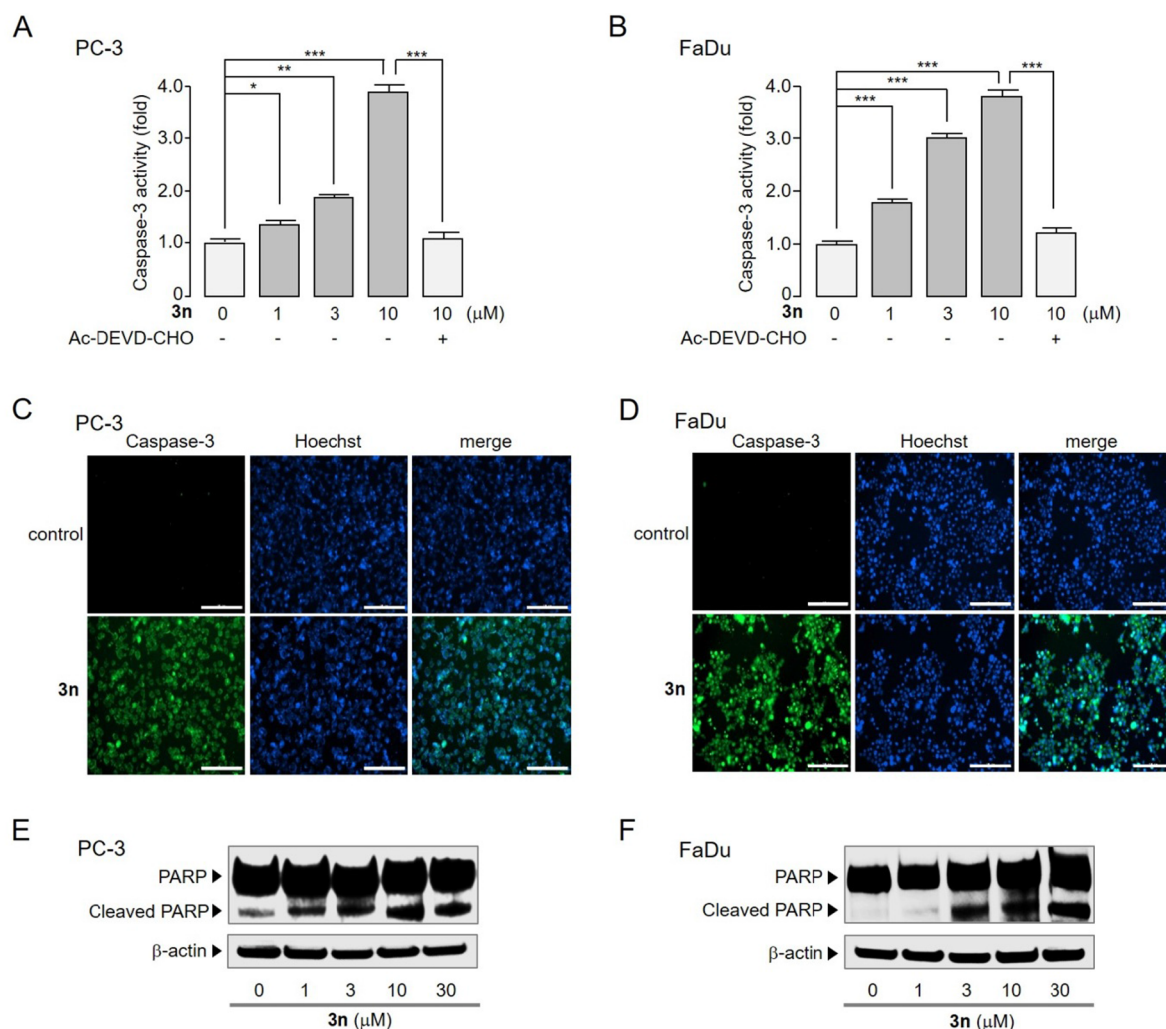


Fig. 4. Effect of **3n** on caspase 3 activity and cleavage of PARP in PC-3 and FaDu cells expressing ANO1. (A-B) Cells were cultured with indicated concentration of **3n** for 12 h, and then 1 μM caspase 3 substrate were treated for 30 min. Caspase 3 was inhibited by 10 μM Ac-DEVD-CHO (mean ± S.E., n = 3). (C-D) Cells were incubated with 10 μM **3n** for 12 h, and then 1 μM caspase 3 substrate and 1 μM Hoechst 33,342 were treated for 30 min. Apoptotic cells were stained with green fluorescence, and nucleus were stained by Hoechst 33,342 (blue). (E-F) Cells were cultured with indicated concentration of **3n** for 12 h, and PARP, cleaved PARP, and β-actin were detected using western blot assay. *P < 0.05 **P < 0.01, ***P < 0.001. (For interpretation of the references to colour in this figure legend, the reader is referred to the web version of this article.)

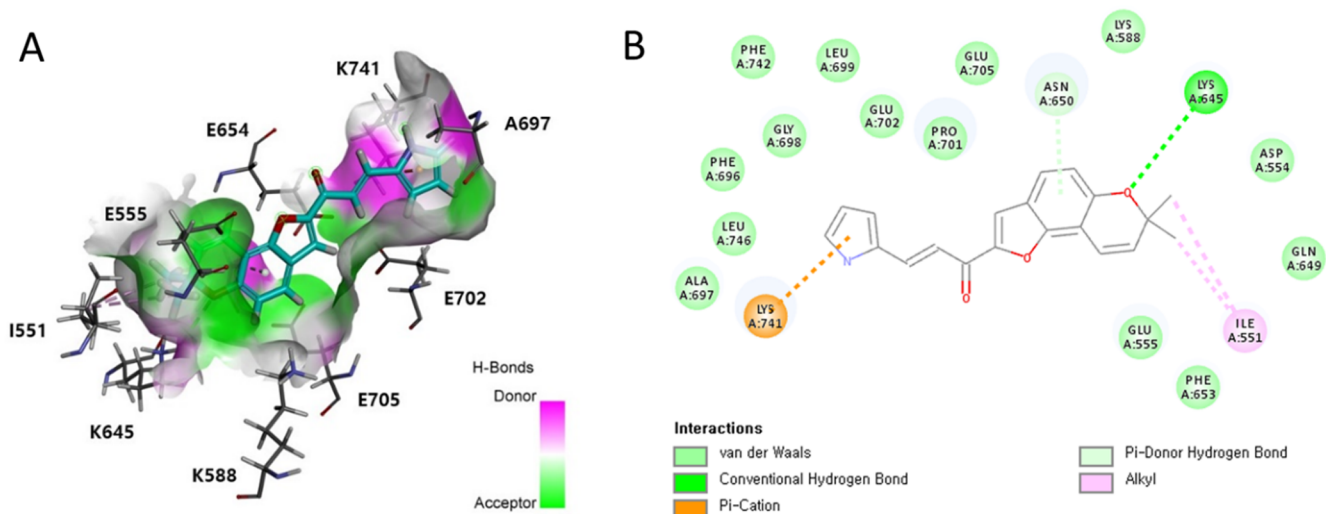
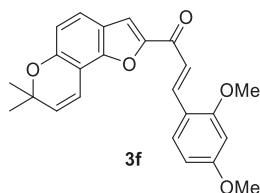
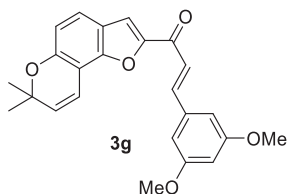


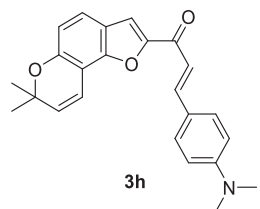
Fig. 5. Molecular docking and binding prediction of **3n** to ANO1. (A) The binding mode between **3n** and the active site of ANO1 shown as a stick model. (B) The chemical binding residues of **3n**-ANO1 were shown in 2D diagram.



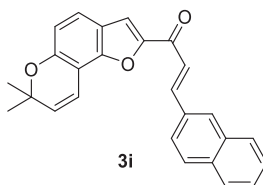
(E)-3-(2,4-Dimethoxyphenyl)-1-(7,7-dimethyl-7H-furo [2,3-f] chromen-2-yl)prop-2-en-1-one (3f). Yellow solid, mp: 121.4–123.1 °C; $^1\text{H NMR}$ (400 MHz, CDCl_3) δ 8.17 (d, $J = 16.0$ Hz, 1H), 7.61 (d, $J = 8.4$ Hz, 1H), 7.55–7.51 (m, 2H), 7.41 (d, $J = 8.8$ Hz, 1H), 6.92 (d, $J = 9.6$ Hz, 1H), 6.81 (d, $J = 8.4$ Hz, 1H), 6.54 (dd, $J = 2.0, 10.0$ Hz, 1H), 6.48–6.48 (m, 1H), 5.72 (d, $J = 10.0$ Hz, 1H), 3.92 (s, 3H), 3.86 (s, 3H), 1.49 (s, 6H); $^{13}\text{C NMR}$ (100 MHz, CDCl_3) δ 179.8, 163.3, 160.7, 154.1, 153.6, 152.4, 139.7, 131.2, 130.4, 122.6, 121.1, 119.8, 117.2, 115.9, 114.7, 113.7, 106.7, 105.6, 98.5, 77.4, 55.7, 55.6, 28.0; **HRMS** (ESI-QTOF) m/z $[\text{M}+\text{Na}]^+$ calcd for $\text{C}_{24}\text{H}_{22}\text{NaO}_5$ 413.1359, found 413.1295.



(E)-3-(3,5-Dimethoxyphenyl)-1-(7,7-dimethyl-7H-furo [2,3-f] chromen-2-yl)prop-2-en-1-one (3g). Yellow solid, mp: 74.5–75.5 °C; $^1\text{H NMR}$ (400 MHz, CDCl_3) δ 7.82 (d, $J = 16.0$ Hz, 1H), 7.57 (s, 1H), 7.48–7.40 (m, 2H), 6.91 (d, $J = 10.0$ Hz, 1H), 6.83–6.81 (m, 3H), 6.53 (s, 1H), 5.72 (d, $J = 10.0$ Hz, 1H), 3.84 (s, 6H), 1.49 (s, 6H); $^{13}\text{C NMR}$ (100 MHz, CDCl_3) δ 178.9, 161.2, 154.0, 153.5, 152.6, 144.1, 136.7, 130.5, 122.8, 121.9, 121.0, 115.7, 115.0, 114.6, 106.6, 106.6, 102.9, 77.3, 55.6, 28.0; **HRMS** (ESI-QTOF) m/z $[\text{M}+\text{Na}]^+$ calcd for $\text{C}_{24}\text{H}_{22}\text{NaO}_5$ 413.1359, found 413.1319.

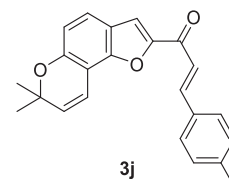


(E)-1-(7,7-Dimethyl-7H-furo [2,3-f] chromen-2-yl)-3-(4-(dimethylamino)-phenyl)prop-2-en-1-one (3h). Orange solid, mp: 172.7–173.8 °C; $^1\text{H NMR}$ (400 MHz, CDCl_3) δ 7.90 (d, $J = 15.2$ Hz, 1H), 7.58 (d, $J = 8.8$ Hz, 2H), 7.52 (s, 1H), 7.41 (d, $J = 8.8$ Hz, 1H), 7.34 (d, $J = 15.2$ Hz, 1H), 6.94 (d, $J = 9.6$ Hz, 1H), 6.81 (d, $J = 8.8$ Hz, 1H), 6.69 (d, $J = 8.8$ Hz, 2H), 5.72 (d, $J = 10.0$ Hz, 1H), 3.05 (s, 6H), 1.49 (s, 6H); $^{13}\text{C NMR}$ (100 MHz, CDCl_3) δ 179.3, 154.3, 153.5, 152.3, 152.2, 145.0, 130.7, 130.4, 122.6, 122.5, 121.2, 116.2, 116.0, 114.6, 113.2, 111.9, 106.7, 77.4, 40.3, 28.0; **HRMS** (ESI-QTOF) m/z $[\text{M}+\text{Na}]^+$ calcd for $\text{C}_{24}\text{H}_{23}\text{NNaO}_3$ 396.1570, found 396.1516.

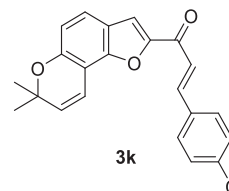


(E)-1-(7,7-Dimethyl-7H-furo [2,3-f] chromen-2-yl)-3-(naphthalen-2-yl)prop-2-en-1-one (3i). Yellow solid, mp: 142.0–143.2 °C; $^1\text{H NMR}$ (400 MHz, CDCl_3) δ 8.10–8.06 (m, 2H), 7.90–7.83 (m, 4H), 7.64–7.61 (m, 2H), 7.55–7.50 (m, 2H), 7.43 (d, $J = 8.4$ Hz, 1H) 6.95 (d,

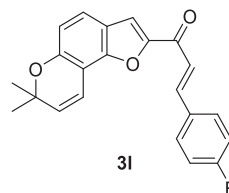
$J = 10.0$ Hz, 1H), 6.84 (d, $J = 8.4$ Hz, 1H), 5.74 (d, $J = 10.0$ Hz, 1H), 1.51 (s, 6H); $^{13}\text{C NMR}$ (100 MHz, CDCl_3) δ 179.0, 154.0, 153.7, 152.6, 144.1, 134.6, 133.5, 132.4, 131.0, 130.5, 128.8, 128.8, 127.9, 127.6, 126.9, 123.8, 122.8, 121.5, 121.0, 115.8, 115.0, 114.5, 106.7, 77.3, 28.0; **HRMS** (ESI-QTOF) m/z $[\text{M}+\text{Na}]^+$ calcd for $\text{C}_{26}\text{H}_{20}\text{NaO}_3$ 403.1305, found 403.1313.



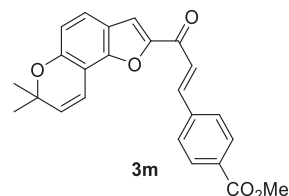
(E)-1-(7,7-Dimethyl-7H-furo [2,3-f] chromen-2-yl)-3-(4-fluorophenyl)prop-2-en-1-one (3j). Yellow solid, mp: 139.4–139.7 °C; $^1\text{H NMR}$ (400 MHz, CDCl_3) δ 7.88 (d, $J = 15.6$ Hz, 1H), 7.67 (t, $J = 6.8$ Hz, 2H), 7.58 (s, 1H), 7.47–7.42 (m, 2H), 7.12 (t, $J = 8.4$ Hz, 2H), 6.92 (d, $J = 10.0$ Hz, 1H), 6.83 (d, $J = 8.4$ Hz, 1H), 5.73 (d, $J = 10.0$ Hz, 1H), 1.48 (s, 6H); $^{13}\text{C NMR}$ (100 MHz, CDCl_3) δ 178.9, 165.5, 163.0, 154.0, 153.6, 152.6, 142.8, 131.1, 130.7, 130.6, 122.8, 121.1, 121.0, 116.4, 116.2, 115.7, 115.1, 114.5, 106.7, 77.3, 28.0; **HRMS** (ESI-QTOF) m/z $[\text{M}+\text{H}]^+$ calcd for $\text{C}_{22}\text{H}_{18}\text{FO}_3$ 349.1234, found 349.1188.



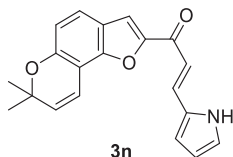
(E)-3-(4-Chlorophenyl)-1-(7,7-dimethyl-7H-furo [2,3-f] chromen-2-yl)prop-2-en-1-one (3k). Yellow solid, mp: 122.6–123.5 °C; $^1\text{H NMR}$ (400 MHz, CDCl_3) δ 7.85 (d, $J = 16.0$ Hz, 1H), 7.60 (d, $J = 8.0$ Hz, 2H), 7.58 (s, 1H), 7.49 (d, $J = 16.0$ Hz, 1H), 7.41 (t, $J = 9.0$ Hz, 3H), 6.91 (d, $J = 10.0$ Hz, 1H), 6.83 (d, $J = 8.4$ Hz, 1H), 5.73 (d, $J = 10.0$ Hz, 1H), 1.49 (s, 6H); $^{13}\text{C NMR}$ (100 MHz, CDCl_3) δ 178.8, 154.1, 153.5, 152.6, 142.6, 136.7, 133.4, 130.6, 129.8, 129.4, 122.8, 121.9, 120.9, 115.7, 115.1, 114.7, 106.7, 77.3, 28.0; **HRMS** (ESI-QTOF) m/z $[\text{M}+\text{H}]^+$ calcd for $\text{C}_{22}\text{H}_{18}\text{ClO}_3$ 365.0939, found 365.0889.



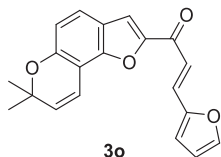
(E)-3-(4-Bromophenyl)-1-(7,7-dimethyl-7H-furo [2,3-f] chromen-2-yl)prop-2-en-1-one (3l). Yellow solid, mp: 145.8–146.2 °C; $^1\text{H NMR}$ (400 MHz, CDCl_3) δ 7.84 (d, $J = 15.6$ Hz, 1H), 7.58–7.49 (m, 6H), 7.43 (d, $J = 8.8$ Hz, 1H), 6.91 (d, $J = 10.0$ Hz, 1H), 6.83 (d, $J = 8.4$ Hz, 1H), 5.73 (d, $J = 10.0$ Hz, 1H), 1.49 (s, 6H); $^{13}\text{C NMR}$ (100 MHz, CDCl_3) δ 178.8, 154.1, 153.5, 152.6, 142.6, 133.8, 132.4, 131.5, 130.6, 130.0, 125.1, 122.8, 122.1, 121.00, 115.7, 115.1, 114.7, 106.7, 77.4, 28.0; **HRMS** (ESI-QTOF) m/z $[\text{M}+\text{Na}]^+$ calcd for $\text{C}_{22}\text{H}_{17}\text{BrNaO}_3$ 431.0253, found 431.0267.



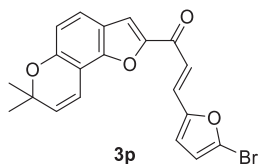
Methyl (E)-4-(3-(7,7-dimethyl-7H-furo [2,3-f] chromen-2-yl)-3-oxoprop-1-en-1-yl)benzoate (3m). Yellow solid, mp: 170.2–172.9 °C; $^1\text{H NMR}$ (400 MHz, CDCl_3) δ 8.10 (d, $J = 8.4$ Hz, 2H), 7.92 (d, $J = 15.6$ Hz, 1H), 7.74 (d, $J = 8.0$ Hz, 1H), 7.61–7.57 (m, 2H), 7.44 (d, $J = 8.4$ Hz, 1H), 6.92 (d, $J = 10.0$ Hz, 1H), 6.84 (d, $J = 8.4$ Hz, 1H), 5.74 (d, $J = 10.0$ Hz, 1H), 3.95 (s, 3H), 1.50 (s, 6H); $^{13}\text{C NMR}$ (100 MHz, CDCl_3) δ 178.7, 166.6, 154.2, 153.5, 152.7, 142.5, 139.1, 131.7, 130.6, 130.3, 128.5, 123.6, 122.9, 121.0, 115.7, 115.2, 115.0, 106.7, 29.9, 28.1; **HRMS** (ESI-QTOF) m/z $[\text{M}+\text{H}]^+$ calcd for $\text{C}_{24}\text{H}_{21}\text{O}_5$ 389.1384, found 389.1371.



(E)-1-(7,7-Dimethyl-7H-furo [2,3-f] chromen-2-yl)-3-(1H-pyrrol-2-yl)prop-2-en-1-one (3n). Brown solid, mp: 116.2–117.1 °C; $^1\text{H NMR}$ (400 MHz, CDCl_3) δ 9.49 (s, 1H), 7.88 (d, $J = 15.6$ Hz, 1H), 7.49 (s, 1H), 7.30 (d, $J = 8.4$ Hz, 1H), 7.22 (d, $J = 15.6$ Hz, 1H), 7.03 (s, 1H), 6.81–6.76 (m, 3H), 6.34 (s, 1H), 5.66 (d, $J = 9.6$ Hz, 1H), 1.46 (s, 6H); $^{13}\text{C NMR}$ (100 MHz, CDCl_3) δ 179.3, 153.9, 153.7, 152.4, 134.0, 130.5, 129.5, 123.8, 122.6, 121.1, 116.0, 115.7, 115.1, 114.8, 113.8, 111.7, 106.6, 77.2, 28.0; **HRMS** (ESI-QTOF) m/z $[\text{M}+\text{H}]^+$ calcd for $\text{C}_{20}\text{H}_{18}\text{NO}_3$ 320.1281, found 320.1234.



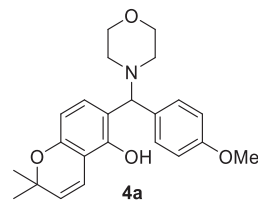
(E)-1-(7,7-Dimethyl-7H-furo [2,3-f] chromen-2-yl)-3-(furan-2-yl)prop-2-en-1-one (3o). Dark yellow solid, mp: 138.4–138.9 °C; $^1\text{H NMR}$ (400 MHz, CDCl_3) δ 7.65 (d, $J = 15.6$ Hz, 1H), 7.55–7.54 (m, 2H), 7.42 (s, 1H), 7.39 (d, $J = 7.2$ Hz, 1H), 6.91 (d, $J = 10.0$ Hz, 1H), 6.81 (d, $J = 8.4$ Hz, 1H), 6.73 (d, $J = 3.2$ Hz, 1H), 6.52–6.51 (m, 1H), 5.71 (d, $J = 9.6$ Hz, 1H), 1.48 (s, 6H); $^{13}\text{C NMR}$ (100 MHz, CDCl_3) δ 178.8, 153.9, 153.6, 152.5, 151.7, 145.2, 130.5, 130.0, 122.7, 121.0, 119.0, 116.7, 115.8, 114.9, 114.4, 112.9, 106.6, 77.3, 28.0; **HRMS** (ESI-QTOF) m/z $[\text{M}+\text{Na}]^+$ calcd for $\text{C}_{20}\text{H}_{16}\text{NaO}_4$ 343.0941, found 343.0995.



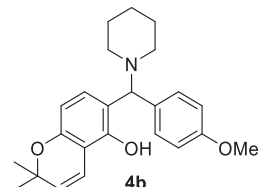
(E)-3-(5-Bromofuran-2-yl)-1-(7,7-dimethyl-7H-furo [2,3-f] chromen-2-yl)prop-2-en-1-one (3p). Brown solid, mp: 112.7–113.7 °C; $^1\text{H NMR}$ (400 MHz, CDCl_3) δ 7.57–7.51 (m, 2H), 7.42–7.34 (m, 2H), 6.92 (d, $J = 10.0$ Hz, 1H), 6.81 (d, $J = 8.4$ Hz, 1H), 6.66 (s, 1H), 6.45 (d, $J = 3.6$ Hz, 1H), 5.72 (d, $J = 10.0$ Hz, 1H), 1.48 (s, 6H); $^{13}\text{C NMR}$ (100 MHz, CDCl_3) δ 178.4, 154.0, 153.6, 153.5, 152.6, 130.5, 128.5, 126.1, 122.8, 121.0, 119.4, 118.6, 115.8, 115.0, 114.8, 114.7, 106.7, 77.3, 28.0; **HRMS** (ESI-QTOF) m/z $[\text{M}+\text{H}]^+$ calcd for $\text{C}_{20}\text{H}_{16}\text{BrO}_4$ 399.0226, found 399.0161.

General procedure for the synthesis of 4: To a solution of 1 (30 mg, 0.15 mmol) in anhydrous dichloromethane (1 mL) were added morpholine (15.2 μL , 1.2 equiv), and 4-methoxyphenylboronic acid (26.8 mg, 1.2 equiv) at room temperature. After being stirred at 60 °C for 18 h, the reaction mixture was diluted with CH_2Cl_2 (2 mL) and washed with H_2O (5 mL). The aqueous layer was extracted with CH_2Cl_2 (1 mL) two more times. The organic layer was dried over MgSO_4 , filtered, and concentrated *in vacuo*. The residue was purified by silica gel column chromatography (*n*-hexane:ethyl acetate:dichloromethane = 30:1:2) to

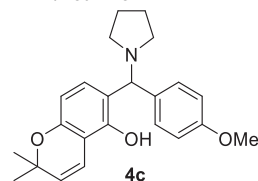
give 4a (52.1 mg, 91%).



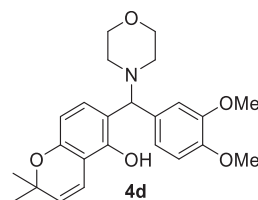
6-((4-Methoxyphenyl)(morpholino)methyl)-2,2-dimethyl-2H-chromen-5-ol (4a). Ivory solid, mp: 99.7–101.3 °C; $^1\text{H NMR}$ (400 MHz, CDCl_3) δ 12.13 (s, 1H), 7.29 (d, $J = 7.6$ Hz, 2H), 6.83 (d, $J = 8.4$ Hz, 2H), 6.74 (d, $J = 9.6$ Hz, 1H), 6.64 (d, $J = 8.4$ Hz, 1H), 6.20 (d, $J = 8.0$ Hz, 1H), 6.64 (d, $J = 8.4$ Hz, 1H), 4.31 (s, 1H), 3.76 (s, 7H), 2.58–2.42 (m, 4H), 1.42 (s, 3H), 1.39 (s, 3H); $^{13}\text{C NMR}$ (100 MHz, CDCl_3) δ 159.3, 153.2, 152.2, 131.4, 129.9, 129.2, 128.5, 117.2, 117.1, 114.2, 110.0, 107.6, 75.8, 75.6, 67.0, 55.3, 52.0, 28.1; **HRMS** (ESI-QTOF) m/z $[\text{M}+\text{K}]^+$ calcd for $\text{C}_{23}\text{H}_{27}\text{KNO}_4$ 420.1572, found 420.1510.



6-((4-Methoxyphenyl)(piperidin-1-yl)methyl)-2,2-dimethyl-2H-chromen-5-ol (4b). Ivory solid, mp: 101.4–102.9 °C; $^1\text{H NMR}$ (400 MHz, CDCl_3) δ 13.10 (s, 1H), 7.27 (s, 1H), 6.84 (d, $J = 8.8$ Hz, 2H), 6.78 (d, $J = 10.0$ Hz, 1H), 6.59 (d, $J = 8.4$ Hz, 1H), 6.17 (d, $J = 8.4$ Hz, 1H), 5.57 (d, $J = 10.0$ Hz, 1H), 4.43 (s, 1H), 3.78 (s, 3H), 2.39 (s, 4H), 1.63 (s, 6H), 1.43 (s, 3H), 1.41 (s, 3H); $^{13}\text{C NMR}$ (100 MHz, CDCl_3) δ 159.1, 153.6, 152.9, 131.1, 130.3, 129.0, 128.2, 117.8, 117.4, 113.9, 109.8, 106.8, 75.7, 75.1, 55.2, 28.0, 27.9, 26.2, 24.2; **HRMS** (ESI-QTOF) m/z $[\text{M}+\text{H}]^+$ calcd for $\text{C}_{24}\text{H}_{30}\text{NO}_3$ 380.2220, found 380.2132.

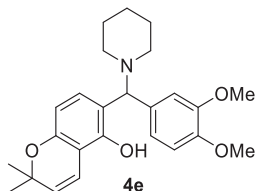


6-((4-Methoxyphenyl)(pyrrolidin-1-yl)methyl)-2,2-dimethyl-2H-chromen-5-ol (4c). Brown solid, mp: 116.8–117.9 °C; $^1\text{H NMR}$ (400 MHz, CDCl_3) δ 12.73 (s, 1H), 7.34 (d, $J = 8.4$ Hz, 2H), 6.81 (d, $J = 8.8$ Hz, 2H), 6.74 (d, $J = 10.0$ Hz, 1H), 6.66 (d, $J = 8.0$ Hz, 1H), 6.17 (d, $J = 8.4$ Hz, 1H), 5.55 (d, $J = 10.0$ Hz, 1H), 4.28 (s, 1H), 3.76 (s, 3H), 2.63 (s, 2H), 2.47 (s, 2H), 1.82 (s, 4H), 1.42 (s, 3H), 1.38 (s, 3H); $^{13}\text{C NMR}$ (100 MHz, CDCl_3) δ 159.0, 152.9, 152.9, 134.6, 129.1, 128.4, 128.1, 119.3, 117.3, 114.0, 110.0, 107.1, 75.8, 74.5, 55.3, 28.1, 27.9, 23.6; **HRMS** (ESI-QTOF) m/z $[\text{M}+\text{H}]^+$ calcd for $\text{C}_{23}\text{H}_{28}\text{NO}_3$ 366.2064, found 366.2005.

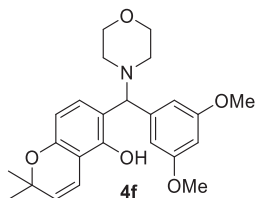


6-((3,4-Dimethoxyphenyl)(morpholino)methyl)-2,2-dimethyl-2H-chromen-5-ol (4d). Ivory solid, mp: 161.2–162.5 °C; $^1\text{H NMR}$ (400 MHz, CDCl_3) δ 12.08 (s, 1H), 6.94 (s, 1H), 6.91 (d, $J = 9.2$ Hz, 1H), 6.77 (d, $J = 8.0$ Hz, 1H), 6.72 (d, $J = 10.0$ Hz, 1H), 6.65 (d, $J = 8.4$ Hz, 1H), 6.19 (d, $J = 8.4$ Hz, 1H), 5.55 (d, $J = 10.0$ Hz, 1H), 4.26 (s, 1H), 3.82 (s, 3H), 3.82 (s, 3H), 3.74 (s, 4H), 2.59 (s, 2H), 2.43 (s, 2H), 1.39 (d,

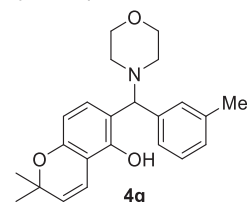
$J = 9.6$ Hz, 6H); ^{13}C NMR (100 MHz, CDCl_3) δ 153.2, 152.2, 149.2, 148.8, 132.0, 129.1, 128.5, 121.1, 117.2, 117.1, 111.1, 110.0, 107.7, 76.1, 75.8, 67.0, 56.0, 55.9, 52.0, 28.0, 27.9; HRMS (ESI-QTOF) m/z [$\text{M} + \text{H}$] $^+$ calcd for $\text{C}_{24}\text{H}_{30}\text{NO}_5$ 412.2118, found 412.2105.



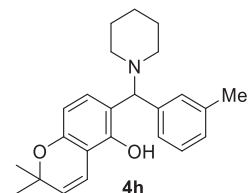
6-((3,4-Dimethoxyphenyl)(piperidin-1-yl)methyl)-2,2-dimethyl-2H-chromen-5-ol (4e). Ivory gum; ^1H NMR (400 MHz, CDCl_3) δ 13.04 (s, 1H), 6.90 (s, 2H), 6.80–6.73 (m, 2H), 6.60 (d, $J = 8.4$ Hz, 1H), 6.16 (d, $J = 8.0$ Hz, 1H), 5.55 (d, $J = 10.0$ Hz, 1H), 4.38 (s, 1H), 3.85 (s, 3H), 3.83 (s, 3H), 2.35 (s, 4H), 1.63 (s, 6H), 1.40 (d, $J = 6.4$ Hz, 6H); ^{13}C NMR (100 MHz, CDCl_3) δ 153.5, 153.0, 149.0, 148.7, 131.8, 129.0, 128.3, 121.5, 117.8, 117.4, 111.0, 109.9, 106.9, 75.8, 75.6, 56.0, 55.9, 52.0, 28.0, 26.2, 24.3; HRMS (ESI-QTOF) m/z [$\text{M} + \text{Na}$] $^+$ calcd for $\text{C}_{25}\text{H}_{31}\text{NNaO}_4$ 432.2145, found 432.2135.



6-((3,5-Dimethoxyphenyl)(morpholino)methyl)-2,2-dimethyl-2H-chromen-5-ol (4f). White solid, mp: 59.4–62.1 °C; ^1H NMR (400 MHz, CDCl_3) δ 11.92 (s, 1H), 6.72 (d, $J = 10.0$ Hz, 1H), 6.67 (d, $J = 8.4$ Hz, 1H), 6.58 (s, 1H), 6.34 (t, $J = 2.2$ Hz, 1H), 6.20 (d, $J = 8.0$ Hz, 1H), 5.55 (d, $J = 10.0$ Hz, 1H), 4.21 (s, 1H), 3.75 (s, 10H), 2.62 (s, 2H), 2.48 (s, 2H), 1.40 (d, $J = 9.2$ Hz, 6H); ^{13}C NMR (100 MHz, CDCl_3) δ 161.1, 153.3, 152.2, 142.0, 129.2, 128.5, 117.2, 116.8, 110.0, 107.7, 106.6, 99.3, 76.7, 75.9, 67.0, 55.4, 52.2, 28.1, 28.0; HRMS (ESI-QTOF) m/z [$\text{M} + \text{Na}$] $^+$ calcd for $\text{C}_{24}\text{H}_{29}\text{NNaO}_4$ 434.1938, found 434.1920.

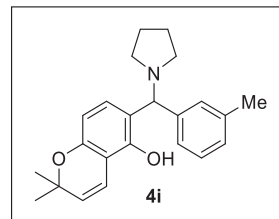


2,2-Dimethyl-6-(morpholino(*m*-tolyl)methyl)-2H-chromen-5-ol (4g). Ivory solid, mp: 58.6–59.5 °C; ^1H NMR (400 MHz, CDCl_3) δ 12.08 (s, 1H), 7.21–7.19 (m, 3H), 7.07 (d, $J = 7.2$ Hz, 1H), 6.75 (d, $J = 10.0$ Hz, 1H), 6.67 (d, $J = 8.4$ Hz, 1H), 6.21 (d, $J = 8.0$ Hz, 1H), 5.58 (d, $J = 10.0$ Hz, 1H), 7.30 (s, 1H), 3.76 (s, 4H), 2.65 (s, 2H), 2.44 (s, 2H), 2.33 (s, 3H), 1.43 (s, 3H), 1.40 (s, 3H); ^{13}C NMR (100 MHz, CDCl_3) δ 153.2, 152.3, 139.4, 138.5, 129.3, 128.9, 128.5, 125.7, 117.2, 117.0, 110.0, 107.7, 76.6, 75.9, 67.0, 52.2, 31.7, 28.1, 28.0, 21.6; HRMS (ESI-QTOF) m/z [$\text{M} + \text{Na}$] $^+$ calcd for $\text{C}_{23}\text{H}_{27}\text{NNaO}_3$ 388.1883, found 388.1871.

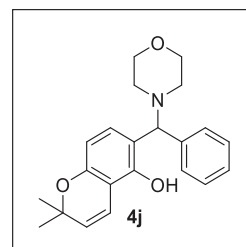


2,2-Dimethyl-6-(piperidin-1-yl(*m*-tolyl)methyl)-2H-chromen-5-ol (4h). Ivory gum; ^1H NMR (400 MHz, CDCl_3) δ 13.0 (s, 1H), 7.21–7.14

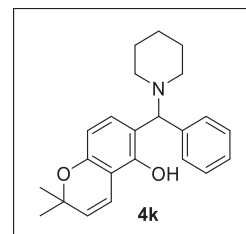
(m, 3H), 7.07 (d, $J = 7.2$ Hz, 1H), 6.76 (d, $J = 10.0$ Hz, 1H), 6.59 (d, $J = 8.4$ Hz, 1H), 5.56 (d, $J = 10.0$ Hz, 1H), 4.39 (s, 1H), 3.03 (s, 4H), 2.33 (s, 3H), 1.63 (s, 6H), 1.42 (s, 3H), 1.40 (s, 3H); ^{13}C NMR (100 MHz, CDCl_3) δ 153.6, 153.0, 139.2, 138.3, 129.1, 128.6, 128.6, 128.3, 117.7, 117.4, 109.9, 106.9, 76.1, 75.8, 29.9, 28.6, 28.1, 28.0, 26.2, 24.3, 21.7; HRMS (ESI-QTOF) m/z [$\text{M} + \text{K}$] $^+$ calcd for $\text{C}_{24}\text{H}_{29}\text{KNO}_2$ 402.1830, found 402.1834.



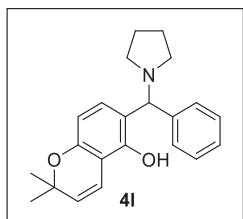
2,2-Dimethyl-6-(pyrrolidin-1-yl(*m*-tolyl)methyl)-2H-chromen-5-ol (4i). Ivory gum; ^1H NMR (400 MHz, CDCl_3) δ 12.73 (s, 1H), 7.26–7.22 (m, 2H), 7.26 (t, $J = 7.4$ Hz, 1H), 7.03 (d, $J = 7.6$ Hz, 1H), 6.74 (d, $J = 10.0$ Hz, 1H), 6.68 (d, $J = 8.4$ Hz, 1H), 6.17 (d, $J = 8.4$ Hz, 1H), 5.55 (d, $J = 10.0$ Hz, 1H), 4.27 (s, 1H), 2.63 (s, 2H), 2.48 (s, 2H), 2.32 (s, 3H), 1.82 (s, 4H), 1.42 (s, 3H), 1.38 (s, 3H); ^{13}C NMR (100 MHz, CDCl_3) δ 153.0, 152.9, 142.3, 138.3, 128.6, 128.6, 128.4, 128.3, 128.2, 125.0, 119.1, 117.5, 109.9, 107.1, 75.8, 75.4, 28.1, 27.9, 23.6, 21.7; HRMS (ESI-QTOF) m/z [$\text{M} + \text{H}$] $^+$ calcd for $\text{C}_{23}\text{H}_{28}\text{NO}_2$ 350.2115, found 350.2042.



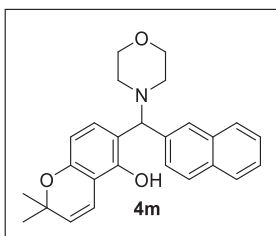
2,2-Dimethyl-6-(morpholino(phenyl)methyl)-2H-chromen-5-ol (4j). White solid, mp: 59.2–61.4 °C; ^1H NMR (400 MHz, CDCl_3) δ 12.06 (s, 1H), 7.39 (s, 2H), 7.31 (t, $J = 7.4$ Hz, 2H), 7.27–7.23 (m, 1H), 6.75 (d, $J = 10.4$ Hz, 1H), 6.67 (d, $J = 8.4$ Hz, 1H), 6.21 (d, $J = 8.4$ Hz, 1H), 5.58 (d, $J = 10.0$ Hz, 1H), 4.34 (s, 1H), 3.75 (s, 4H), 2.62 (s, 2H), 2.44 (s, 2H), 1.43 (s, 3H), 1.40 (s, 3H); ^{13}C NMR (100 MHz, CDCl_3) δ 153.3, 152.2, 139.4, 129.3, 128.9, 128.7, 128.6, 128.1, 117.1, 117.0, 110.0, 107.7, 76.5, 75.9, 67.0, 52.1, 28.1; HRMS (ESI-QTOF) m/z [$\text{M} + \text{Na}$] $^+$ calcd for $\text{C}_{22}\text{H}_{25}\text{NNaO}_3$ 374.1727, found 374.1674.



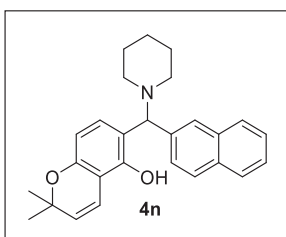
2,2-Dimethyl-6-(phenyl(piperidin-1-yl)methyl)-2H-chromen-5-ol (4k). Ivory solid, mp: 46.7–48.1 °C; ^1H NMR (400 MHz, CDCl_3) δ 12.98 (s, 1H), 7.35 (s, 1H), 7.32–7.24 (m, 4H), 6.76 (d, $J = 10.0$ Hz, 1H), 6.59 (d, $J = 8.0$ Hz, 1H), 6.16 (d, $J = 8.4$ Hz, 1H), 5.56 (d, $J = 10.0$ Hz, 1H), 4.43 (s, 1H), 2.43 (s, 4H), 1.63 (s, 6H), 1.42 (s, 3H), 1.40 (s, 3H); ^{13}C NMR (100 MHz, CDCl_3) δ 153.5, 153.0, 139.3, 129.1, 128.7, 128.3, 127.9, 117.6, 117.4, 109.9, 107.0, 76.0, 75.8, 29.9, 28.1, 28.0, 26.2, 24.3; HRMS (ESI-QTOF) m/z [$\text{M} + \text{H}$] $^+$ calcd for $\text{C}_{23}\text{H}_{28}\text{NO}_2$ 350.2115, found 350.2045.



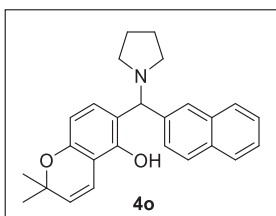
2,2-Dimethyl-6-(phenyl(pyrrolidin-1-yl)methyl)-2H-chromen-5-ol (4l). Yellow gum; $^1\text{H NMR}$ (400 MHz, CDCl_3) δ 12.73 (s, 1H), 7.44 (d, $J = 7.2$ Hz, 2H), 7.30–7.20 (m, 3H), 6.75 (d, $J = 10.0$ Hz, 1H), 6.68 (d, $J = 8.4$ Hz, 1H), 6.18 (d, $J = 8.4$ Hz, 1H), 5.56 (d, $J = 10.0$ Hz, 1H), 4.31 (s, 1H), 2.64 (s, 2H), 2.49 (s, 2H), 1.86–1.79 (m, 4H), 1.43 (s, 3H), 1.38 (s, 3H); $^{13}\text{C NMR}$ (100 MHz, CDCl_3) δ 153.0, 152.8, 142.4, 128.8, 128.4, 128.1, 127.9, 127.7, 119.1, 110.0, 107.2, 75.8, 75.4, 53.2, 28.1, 27.9, 23.6; **HRMS** (ESI-QTOF) m/z $[\text{M}+\text{K}]^+$ calcd for $\text{C}_{22}\text{H}_{25}\text{KNO}_2$ 374.1517, found 374.1675.



2,2-Dimethyl-6-(morpholino(naphthalen-2-yl)methyl)-2H-chromen-5-ol (4m). White solid, mp: 146.7–147.4 °C; $^1\text{H NMR}$ (400 MHz, CDCl_3) δ 12.20 (s, 1H), 7.84–7.78 (m, 4H), 7.62 (d, $J = 6.4$ Hz, 1H), 7.51–7.45 (m, 2H), 8.61 (dd, $J = 4.4, 9.6$ Hz, 1H), 6.74 (d, $J = 8.4$ Hz, 1H), 6.24 (dd, $J = 3.6, 8.0$ Hz, 1H), 5.61 (d, $J = 10.0$ Hz, 1H), 4.52 (s, 1H), 3.77 (s, 4H), 2.68 (s, 2H), 2.48 (s, 2H), 1.46 (s, 3H), 1.41 (s, 1H); $^{13}\text{C NMR}$ (100 MHz, CDCl_3) δ 153.3, 152.2, 137.2, 133.4, 133.1, 129.4, 129.0, 128.6, 128.0, 127.7, 126.4, 126.3, 125.9, 117.1, 116.8, 110.1, 107.8, 76.7, 75.9, 67.0, 52.3, 28.1, 27.9; **HRMS** (ESI-QTOF) m/z $[\text{M}+\text{K}]^+$ calcd for $\text{C}_{26}\text{H}_{27}\text{KNO}_3$ 440.1623, found 440.1529.

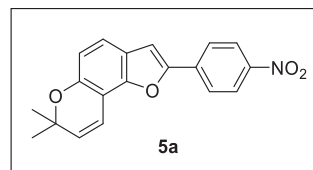


2,2-Dimethyl-6-(naphthalen-2-yl(piperidin-1-yl)methyl)-2H-chromen-5-ol (4n). White solid, mp: 145.9–146.7 °C; $^1\text{H NMR}$ (400 MHz, CDCl_3) δ 13.11 (s, 1H), 7.84–7.76 (m, 4H), 7.59 (s, 1H), 7.50–7.44 (m, 2H), 6.81 (d, $J = 10.0$ Hz, 1H), 6.66 (d, $J = 8.4$ Hz, 1H), 6.17 (d, $J = 8.0$ Hz, 1H), 5.59 (d, $J = 10.0$ Hz, 1H), 4.61 (s, 1H), 2.52 (s, 6H), 1.65 (s, 4H), 1.44 (s, 3H), 1.41 (s, 3H); $^{13}\text{C NMR}$ (100 MHz, CDCl_3) δ 153.5, 153.1, 137.1, 133.4, 133.1, 129.2, 128.6, 128.3, 128.1, 128.0, 127.7, 126.3, 126.2, 117.5, 117.4, 110.0, 107.1, 76.3, 75.8, 29.9, 28.1, 28.0, 26.2, 24.2; **HRMS** (ESI-QTOF) m/z $[\text{M}+\text{H}]^+$ calcd for $\text{C}_{27}\text{H}_{30}\text{NO}_2$ 400.2271, found 400.2183.



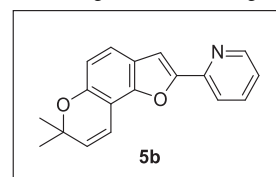
2,2-Dimethyl-6-(naphthalen-2-yl(pyrrolidin-1-yl)methyl)-2H-chromen-5-ol (4o). Ivory solid, mp: 148.1–149.4 °C; $^1\text{H NMR}$ (400 MHz, CDCl_3) δ 12.88 (s, 1H), 7.81 (t, $J = 7.4$ Hz, 2H), 7.77 (d, $J = 6.8$ Hz, 2H), 7.67 (d, $J = 8.4$ Hz, 1H), 7.48–7.42 (m, 2H), 6.79 (d, $J = 9.6$ Hz, 1H), 6.74 (d, $J = 8.0$ Hz, 1H), 6.19 (d, $J = 8.4$ Hz, 1H), 5.58 (d, $J = 10.0$ Hz, 1H), 4.50 (s, 1H), 2.70 (s, 2H), 2.52 (s, 2H), 1.84 (s, 4H), 1.44 (s, 3H), 1.38 (s, 3H); $^{13}\text{C NMR}$ (100 MHz, CDCl_3) δ 153.1, 152.9, 140.0, 133.4, 133.0, 128.8, 128.4, 128.3, 128.1, 127.7, 126.6, 126.2, 126.0, 125.8, 118.8, 117.3, 110.0, 107.3, 75.8, 75.6, 53.3, 29.9, 28.1, 27.9, 23.6; **HRMS** (ESI-QTOF) m/z $[\text{M}+\text{H}]^+$ calcd for $\text{C}_{26}\text{H}_{28}\text{NO}_2$ 386.2115, found 386.2037.

Synthesis of 5a: To a solution of **1** (60 mg, 0.15 mmol) in anhydrous *N,N*-dimethylformamide (1 mL) were added 4-nitrophenyl bromide (69.8 mg, 1.1 equiv) and potassium *tert*-butoxide (49.4 mg, 1.5 equiv) at room temperature. After being stirred at 160 °C for 20 h, the reaction mixture was quenched with water (5 mL) and extracted with ethyl acetate (2 mL). The aqueous layer was extracted with ethyl acetate (1 mL) five more times. The organic layer was dried over MgSO_4 , filtered, and concentrated *in vacuo*. The residue was purified by silica gel column chromatography (*n*-hexane:ethyl acetate:dichloromethane = 50:1:2) to give **5a** (81.1 mg, 87%).



7,7-Dimethyl-2-(4-nitrophenyl)-7H-furo[2,3-f]chromene (5a). Yellow solid, mp: 141.8–142.9 °C; $^1\text{H NMR}$ (400 MHz, CDCl_3) δ 8.29 (d, $J = 8.8$ Hz, 2H), 7.93 (d, $J = 8.8$ Hz, 2H), 7.33 (d, $J = 8.4$ Hz, 1H), 7.15 (s, 1H), 6.87 (d, $J = 9.6$ Hz, 1H), 6.78 (d, $J = 8.4$ Hz, 1H), 5.75 (d, $J = 9.6$ Hz, 1H), 1.50 (s, 6H); $^{13}\text{C NMR}$ (100 MHz, CDCl_3) δ 152.6, 151.9, 151.7, 146.9, 136.6, 130.9, 124.6, 124.5, 122.3, 121.0, 115.8, 113.9, 107.0, 106.5, 105.8, 27.9; **HRMS** (ESI-QTOF) m/z $[\text{M}+\text{Na}]^+$ calcd for $\text{C}_{19}\text{H}_{15}\text{NNaO}_4$ 344.0893, found 344.0893.

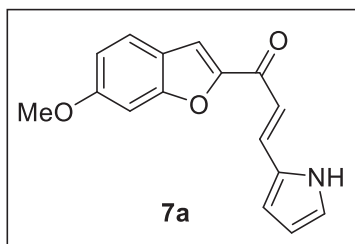
Synthesis of 5b: To a solution of **1** (60 mg, 0.30 mmol) in anhydrous *N,N*-dimethylformamide (1.1 mL) were added 2-(chloromethyl)pyridine hydrochloride (49.6 mg, 1 equiv) and potassium carbonate (125.3 mg, 3 equiv) at room temperature. After being stirred at 50 °C for 11 h, the reaction mixture was quenched with water (5 mL) and extracted with ethyl acetate (2 mL). The aqueous layer was extracted with ethyl acetate (1 mL) five more times. The organic layer was dried over MgSO_4 , filtered, and concentrated *in vacuo* to give the crude residue. To a vial charged with the crude residue in anhydrous *N,N*-dimethylformamide (1 mL) was added potassium *tert*-butoxide (43.3 mg, 1.5 equiv) at room temperature. After being stirred at 80 °C for 16 h, the reaction mixture was quenched with water (5 mL) and extracted with ethyl acetate (2 mL). The aqueous layer was extracted with ethyl acetate (1 mL) five more times. The organic layer was dried over MgSO_4 , filtered, and concentrated *in vacuo*. The residue was purified by silica gel column chromatography (*n*-hexane:ethyl acetate:dichloromethane = 10:1:2) to give **5b** (44.8 mg, 55%).



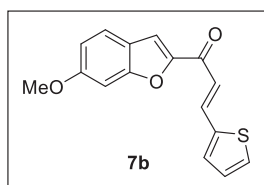
2-(7,7-Dimethyl-7H-furo[2,3-f]chromen-2-yl)pyridine (5b). Ivory solid, mp: 59.7–61.3 °C; $^1\text{H NMR}$ (400 MHz, CDCl_3) δ 8.65 (d, $J = 4.8$ Hz, 1H), 7.85 (d, $J = 7.6$ Hz, 1H), 7.76 (t, $J = 7.8$ Hz, 1H), 7.36–7.33 (m, 2H), 7.21–7.18 (m, 1H), 6.91 (d, $J = 9.6$ Hz, 1H), 6.77 (d, $J = 8.4$ Hz, 1H), 5.73 (d, $J = 10.0$ Hz, 1H), 1.49 (s, 6H); $^{13}\text{C NMR}$

(100 MHz, CDCl₃) 154.5, 151.5, 151.4, 150.0, 149.6, 136.8, 130.6, 122.5, 121.1, 119.4, 116.1, 113.5, 106.6, 105.3, 76.6, 27.9; **HRMS** (ESI-QTOF) m/z [M+Na]⁺ calcd for C₁₈H₁₅NNaO₂ 300.0995, found 300.0924.

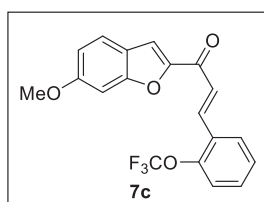
General procedure for the synthesis of 7: To a solution of 2-hydroxy-4-methoxybenzaldehyde (300 mg, 1.97 mmol, 1.0 equiv) in acetonitrile (6.6 mL) were added chloroacetone (190.36 μ l, 1.2 equiv) and potassium carbonate (817.54 mg, 3.0 equiv) at room temperature. After being stirred at 130 °C for 16 h, the reaction mixture was concentrated *in vacuo* and the crude residue was extracted with ethyl acetate (5 mL \times 3) three times. The organic layer was dried over MgSO₄, filtered, and concentrated *in vacuo* to give the crude residue. The residue was purified by silica gel column chromatography (*n*-hexane:ethyl acetate:dichloromethane = 50:1:2) to give **6** (354.4 mg, 95%). To a vial charged with **6** (30 mg, 0.16 mmol) and pyrrole-2-carboxaldehyde (18 mg, 1.2 equiv) in ethanol (1 mL) was added K₂CO₃ (1.0 equiv) at room temperature. After being stirred at 60 °C for 3 h, the reaction mixture was concentrated under reduced pressure, extracted with CH₂Cl₂ (2 mL), and washed with H₂O (5 mL). The water layer was extracted with CH₂Cl₂ (1 mL) two more times. The organic layer was dried over MgSO₄, filtered, and concentrated *in vacuo*. The residue was purified by silica gel column chromatography (*n*-hexane:ethyl acetate:dichloromethane = 15:1:2) to give **7a** (25.7 mg, 62%).



(E)-1-(6-Methoxybenzofuran-2-yl)-3-(1H-pyrrol-2-yl)prop-2-en-1-one (7a). Yellow solid, mp: 176.6–177.2 °C; ¹H NMR (400 MHz, CDCl₃) δ 9.02 (s, 1H), 7.85 (d, J = 15.6 Hz, 1H), 7.50–7.56 (m, 2H), 7.18 (d, J = 15.6 Hz, 1H), 7.00–7.07 (m, 2H), 6.94 (dd, J = 2.2, 8.6 Hz, 1H), 6.74–6.78 (m, 1H), 6.33–6.38 (m, 1H), 3.87 (s, 3H); ¹³C NMR (100 MHz, CDCl₃) δ 178.9, 160.8, 157.2, 153.7, 133.6, 129.3, 123.4, 123.4, 120.7, 115.8, 114.9, 114.1, 112.9, 111.6, 95.6, 55.7; **HRMS** (ESI-QTOF) m/z [M+H]⁺ calcd for C₁₆H₁₄NO₃ 268.0968, found 268.1017.



(E)-1-(6-Methoxybenzofuran-2-yl)-3-(thiophen-2-yl)prop-2-en-1-one (7b). Pale yellow solid, mp: 127.0–127.7 °C; ¹H NMR (400 MHz, CDCl₃) δ 8.03 (d, J = 15.6 Hz, 1H), 7.55–7.60 (m, 2H), 7.44 (d, J = 5.2 Hz, 1H), 7.38 (d, J = 3.6 Hz, 1H), 7.30 (d, J = 15.6 Hz, 1H), 7.06–7.12 (m, 2H), 6.95 (dd, J = 2.2, 8.6 Hz, 1H), 3.89 (s, 3H); ¹³C NMR (100 MHz, CDCl₃) δ 178.5, 161.1, 157.4, 153.3, 140.3, 136.4, 132.3, 129.0, 128.4, 123.5, 120.6, 120.1, 114.4, 113.7, 95.6, 55.7; **HRMS** (ESI-QTOF) m/z [M+H]⁺ calcd for C₁₆H₁₃O₃S 285.0580, found 285.0605.



(E)-1-(6-Methoxybenzofuran-2-yl)-3-(2-(trifluoromethoxy)phenyl)prop-2-en-1-one (7c). Yellow solid, mp: 75.0–76.0 °C; ¹H NMR (400 MHz, CDCl₃) δ 8.12 (d, J = 16.0 Hz, 1H), 7.82 (d, J = 7.6 Hz, 1H), 7.55–7.64 (m, 3H), 7.46 (t, J = 7.6 Hz, 1H), 7.31–7.40 (m, 2H), 7.09 (s, 1H), 6.97 (dd, J = 2.0, 8.8 Hz, 1H), 3.90 (s, 3H); ¹³C NMR (100 MHz, CDCl₃) δ 198.7, 178.6, 161.3, 157.5, 153.2, 148.0, 136.7, 131.5, 128.7, 128.1, 127.1, 124.3, 123.6, 121.4, 120.5, 114.5, 114.2, 95.6; **HRMS** (ESI-QTOF) m/z [M+H]⁺ calcd for C₁₉H₁₄F₃O₄ 363.0839, found 363.0922.

4.2. Bioassay

4.2.1. Cell culture

Fisher rat thyroid (FRT) cells stably expressing ANO1, ANO2 and CFTR were established as described previously [46]. FRT cells were cultured in Coon's modified F12 medium supplemented with 10% FBS, 2 mM L-glutamine, 100 units/mL penicillin and 100 μ g/mL streptomycin. Prostate cancer cells (PC-3) and hypopharyngeal cancer cells (FaDu) were cultured in RPMI1640 medium containing 10% FBS, 100 units/ml penicillin and 100 μ g/ml streptomycin.

4.2.2. Construction of ANO1-knock out (KO) cells

PLentiCRISPRv2 vector containing ANO1 CRISPR Guide RNA (CCTGATGCCGAGTGCAAGTA) and Cas9 (Clone ID: X35909) was purchased from Genescript (Piscataway, NJ, USA). The DNA composed of 150 ng CRISPR/Cas9 with ANO1 gRNA, 1200 ng packaging plasmid (pPAX2) and 400 ng envelope plasmid (pMD2.G) were co-transfected in HEK293T cells on 6 well plate. After 48 h, supernatant containing lentivirus particles were collected and filtered by 0.45 μ m syringe filter. The lentiviral particle with medium (1:1 mixture) were treated with cells on 24 well plate for 72 h. ANO1-knockout cells were selected by puromycin (Sigma-Aldrich).

4.2.3. YFP fluorescence quenching analysis

FRT cells stably expressing YFP-H148Q/I152L/F46L and ANO1, ANO2 or CFTR were plated in 96-well plates at 2×10^3 cells per well and incubated for 48 h. The 96-well plates were washed twice with 300 μ l PBS and 100 μ l PBS was left, and test compounds were treated for 20 min. The 96-well plates were transferred to a microplate reader and YFP fluorescence measurements were performed. To measure the ANO1-, ANO2- or CFTR-mediated Γ influx, 100 μ l of 70 mM Γ solution containing 200 μ M ATP or 10 μ M forskolin was injected at 1 or 2 s, fluorescence was measured once every 0.4 s and continuous for 5–6 s. The inhibitory effect of the test compound was measured by calculating the initial slope of YFP fluorescence reduction by Γ influx. Analysis were performed using FLUOstar Omega microplate reader and MARS Data Analysis Software (BMG Labtech).

4.2.4. Western blot analysis

Western blotting proceeded as previously reported [46]. PC3 and FaDu cells were lysed in ice-cold lysis buffer (50 mM Tris-HCl (pH 7.4), 1 mM EDTA, 1 mM Na₃VO₄, 150 mM NaCl, 1% Nonidet P-40, 0.25% sodium deoxycholate protease inhibitor mixture). Total cell lysates were centrifuged at 13,000 rpm for 15 min at 4 °C and protein concentration were determined with a Bradford assay kit (Thermo Fisher Scientific) according to the manufacturer's instructions. The supernatant protein was separated via 4–12% Tris-glycine precast gel (KOMA BIOTECH), and transferred to a PVDF membrane and then blocked with 5% Bovine Serum Albumin (BSA) in Tris-buffered saline containing 0.1% Tween 20 (TBST) for 1 h. Membranes were then incubated with anti-ANO1 antibody (Abcam), anti-cleaved PARP (BD Biosciences) and beta-actin (Santa Cruz Biotechnology). Next, the membranes were incubated with HRP-conjugated anti-secondary IgG antibody (Enzo life science) and visualized using the ECL Plus western blotting detection system (GE Healthcare).

4.2.5. Cell viability assay

MTS analysis was performed on CellTiter 96® Aqueous One Solution Cell Proliferation Assay kit (Promega). Briefly, PC3 and FaDu cells were plated in 96-well plates and incubated with 3% FBS containing medium for 24 h. Once the cells reached ~20% confluency, the cells were treated with test compound for 48 h. Then, the medium and compound were exchanged every 24 h. After removing the cell culture medium, MTS solution was added to the 96-well plate and re-incubated for 1 h. Absorbance of formazan was measured by Infinite M200 microplate reader (Tecan) at 490 nm.

4.2.6. Caspase 3 activity assay

PC-3 and FaDu cells were cultured in 96-well cell culture plate about 30% confluence, test compound and Ac-DEVD-CHO, a caspase-3 inhibitor, were treated for 24 h. To measure caspase-3 activity, the cell culture medium was replaced with PBS containing 1 μM NucView 488 caspase-3 substrate, and the cells were incubated at room temperature for 30 min and then stained with 1 μM Hoechst 33342. The fluorescence intensity of NucView 488 and Hoechst 33,342 were measured using FLUOstar Omega microplate reader (BMG Labtech) and fluorescence microscopy images were obtained with Lionheart FX automated live cell microscope (BioTek).

4.2.7. Molecular docking analysis

The structure of ANO1 was obtained from the Protein data bank (PDB ID: 5OYB) [72]. **3n** were docked using the CHARMM force field in Discovery Studio software on the binding site of ANO1 [74]. For the docking analysis, the binding site was defined within 10.7 Å sphere centered from the result of 3D-QSAR analysis [73]. Based on the docking results, *in situ* minimization and ligand conformational entropy were determined to calculate binding energy of the most predictive binding mode.

4.3. Statistical analysis

The results of multiple experiments are presented as the means ± S.E. Statistical analysis was performed with Student's *t*-test or by analysis of variance as appropriate. A value of *P* < 0.05 was considered statistically significant. Dose-response curve and IC₅₀ values were calculated using GraphPad Prism Software.

Acknowledgements

We thank the National Research Foundation of Korea (NRF-2017R1A2A2A05069364, NRF-2018R1A6A1A03023718, NRF-2019R111A1A01061117, and NRF-2020R1A2C2005961) for generous financial support. This research was supported (in part) by Yonsei University Research Fund (Post Doc. Researcher Supporting Program) of 2019 (project no.: 2019-12-0013).

Appendix A. Supplementary material

Supplementary data to this article can be found online at <https://doi.org/10.1016/j.bioorg.2020.104000>.

References

- Costa, T.A. Dias, A. Brito, F. Proença, Biological importance of structurally diversified chromenes, *Eur. J. Med. Chem.* 123 (2016) 487–507.
- Boyd, A. Han, Deguelin and its role in chronic diseases, *Adv. Exp. Med. Biol.* 929 (2016) 363–375.
- Z.Q. Xu, M.T. Flavin, T.R. Jenta, Calanolides, the naturally occurring anti-HIV agents, *Curr. Opin. Drug. Discov. Devel.* 3 (2000) 155–166.
- A.D. Patil, A.J. Freyer, D.S. Eggleston, R.C. Haltiwanger, B. Tomcowicz, A. Breen, R.K. Johnson, Daleformis, a new phytoalexin from the roots of *Dalea filiciformis*: An inhibitor of endothelin converting enzyme, *J. Nat. Prod.* 60 (1997) 306–308.
- Y. Hano, Y. Yamagami, M. Kobayashi, R. Isohata, T. Nomura, Artonins E and F, two new prenylflavones from the bark of *Artocarpus communis* Forst, *Heterocycles* 31

- (1990) 877–882.
- Y.Q. Guo, G.H. Tang, L.L. Lou, W. Li, B. Zhang, B. Liu, S. Yin, Prenylated flavonoids as potent phosphodiesterase-4 inhibitors from *Morus alba*: Isolation, modification, and structure-activity relationship study, *Eur. J. Med. Chem.* 144 (2018) 758–766.
- M.A. Arai, F. Ochi, Y. Makita, T. Chiba, K. Higashi, A. Suganami, Y. Tamura, T. Toida, A. Iwama, S.K. Sadhu, F. Ahmed, M. Ishibashi, GLII Inhibitors Identified by Target Protein Oriented Natural Products Isolation (TPO-NAPI) with Hedgehog Inhibition, *ACS Chem. Biol.* 13 (2018) 2551–2559.
- H. An, S. Lee, J. Lee, D.H. Jo, J. Kim, Y.-S. Jeong, M.J. Heo, C.S. Cho, H. Choi, J.H. Seo, S. Hwang, J. Lim, T. Kim, H.O. Jun, J. Sim, C. Lim, J. Hur, J. Ahn, H.S. Kim, S.-Y. Seo, Y. Na, S.-H. Kim, J. Lee, J. Lee, S.-J. Chung, Y.-M. Kim, K.-W. Kim, S.G. Kim, J.H. Kim, Y.-G. Suh, Novel Hypoxia-Inducible Factor 1α (HIF-1α) inhibitors for angiogenesis-related ocular diseases: discovery of a novel scaffold via ring-truncation strategy, *J. Med. Chem.* 61 (2018) 9266–9286.
- B. Lin, J.-F. Huang, X.-W. Liu, X.-T. Ma, X.-L. Liu, Y. Lu, Y. Zhou, F.M. Guo, T.T. Feng, Rapid, microwave-accelerated synthesis and anti-osteoporosis activities evaluation of morusin scaffolds and morusignin L scaffolds, *Bioorg. Med. Chem. Lett.* 27 (2017) 2389–2396.
- H.S. Kim, M. Hong, S.-C. Lee, H.-Y. Lee, Y.-G. Suh, D.-C. Oh, J.H. Seo, H. Choi, J.Y. Kim, K.-W. Kim, J.H. Kim, J. Kim, Y.-M. Kim, S.-J. Park, H.-J. Park, J. Lee, Ring-truncated deguelin derivatives as potent Hypoxia Inducible Factor-1α (HIF-1α) inhibitors, *Eur. J. Med. Chem.* 104 (2015) 157–164.
- H.S. Kim, V.-H. Hoang, M. Hong, K.C. Kim, J. Ann, C.-T. Nguyen, J.H. Seo, H. Choi, J.Y. Kim, K.-W. Kim, W.S. Byun, S. Lee, S. Lee, Y.-G. Suh, J. Chen, H.-J. Park, T.-M. Cho, J.Y. Kim, J.H. Seo, J. Lee, Investigation of B, C-ring truncated deguelin derivatives as heat shock protein 90 (HSP90) inhibitors for use as anti-breast cancer agents, *Bioorg. Med. Chem.* 27 (2019) 1370–1381.
- S. Oh, H.J. Jang, S.K. Ko, Y. Ko, S.B. Park, Construction of a polyheterocyclic benzopyran library with diverse core skeletons through diversity-oriented synthesis pathway, *J. Comb. Chem.* 12 (2010) 548–558.
- K.C. Nicolaou, J.A. Pfefferkorn, A.J. Roecker, G.Q. Cao, S. Barluenga, H.J. Mitchell, Natural product-like combinatorial libraries based on privileged structures. 1. general principles and solid-phase synthesis of benzopyrans, *J. Am. Chem. Soc.* 122 (2000) 9939–9953.
- K.C. Nicolaou, J.A. Pfefferkorn, H.J. Mitchell, A.J. Roecker, S. Barluenga, G.Q. Cao, R.L. Affleck, J.E. Lillig, Natural product-like combinatorial libraries based on privileged structures. 2. construction of a 10,000-membered benzopyran library by directed split-and-pool chemistry using NanoKans and optical encoding, *J. Am. Chem. Soc.* 122 (2000) 9954–9967.
- K. Passador, S. Thorimbert, C. Botuha, Heteroaromatic rings of the Future: exploration of unconquered chemical space, *Synthesis* 51 (2019) 384–398.
- J.-L. Reymond, M. Awale, Exploring chemical space for drug discovery using the chemical universe database, *ACS Chem. Neurosci.* 3 (2012) 649–657.
- C.M. Dobson, Chemical space and biology, *Nature* 432 (2004) 824–828.
- R.S. Bohacek, C. McMartin, W.C. Guida, The art and practice of structure-based drug design: a molecular modeling perspective, *Med. Res. Rev.* 16 (1996) 3–50.
- M. Srinivas Lavanya Kumar, J. Singh, S.K. Manna, S. Maji, R. Konwar, G. Panda, Diversity oriented synthesis of chromene-xanthene hybrids as anti-breast cancer agents, *Bioorg. Med. Chem. Lett.* 28 (2018) 778–782.
- N. Luise, P.G. Wyatt, Generation of polar semi-saturated bicyclic pyrazoles for fragment-based drug-discovery campaigns, *Chemistry (Easton)* 24 (2018) 10443–10451.
- J. Halder, D. Das, S. Nanda, A distinctive transformation based diversity oriented synthesis of small ring carbocycles and heterocycles from biocatalytically derived enantiopure alpha-substituted-beta-hydroxyesters, *Org. Biomol. Chem.* 16 (2018) 2549–2575.
- M.L.N. Rao, V.N. Murty, S. Nand, Functional group manoeuvring for tuning stability and reactivity: synthesis of cicerfuran, moracins (D, E, M) and chromene-fused benzofuran-based natural products, *Org. Biomol. Chem.* 15 (2017) 9415–9423.
- L. Herrera, P. Barrio, I. Ibáñez, R. Román, N. Mateu, S. Fustero, 8-Iodonaphthalene-1-carbaldehyde: A versatile building block for diversity-oriented synthesis, *Org. Lett.* 18 (2016) 4722–4725.
- J. Kim, M. Park, J. Choi, D.K. Singh, H.J. Kwon, S.H. Kim, I. Kim, Design, synthesis, and biological evaluation of novel pyrrolo[1,2-*a*]pyrazine derivatives, *Bioorg. Med. Chem. Lett.* 29 (2019) 1350–1356.
- A. Dagar, G.H. Bae, J.H. Lee, I. Kim, Tandem [4+1+1] annulation approach to 4-acyl-3,4-dihydropyrrolo[1,2-*a*]pyrazines: diastereoselective construction of dihydropyrazine units from Pyrroles, *J. Org. Chem.* 84 (2019) 6916–6927.
- S. Park, E.H. Kim, J. Kim, S.H. Kim, I. Kim, Biological evaluation of indolizine-chalcone hybrids as new anticancer agents, *Eur. J. Med. Chem.* 144 (2018) 435–443.
- M. Nayak, D.K. Singh, I. Kim, Regiospecific synthesis of 5- and 6-acylated naphtho [1,2-*b*]benzofurans via intramolecular alkyne carbonyl metathesis, *Synthesis* 49 (2017) 2063–2073.
- S.H. Moon, Y. Jung, S.H. Kim, I. Kim, Synthesis, characterization and biological evaluation of anti-cancer indolizine derivatives via inhibiting beta-catenin activity and activating p53, *Bioorg. Med. Chem. Lett.* 26 (2016) 110–113.
- Y. Jung, I. Kim, Deformylative intramolecular hydroarylation: Synthesis of Benzo[*e*]pyrido[1,2-*a*]indoles, *Org. Lett.* 17 (2015) 4600–4603.
- M. Kim, Y. Jung, I. Kim, Domino Knoevenagel condensation/intramolecular aldol cyclization route to diverse indolizines with densely functionalized pyridine units, *J. Org. Chem.* 78 (2013) 10395–10404.
- I. Kim, K. Kim, Expedient synthesis of highly substituted indolizines via a palladium-catalyzed domino sequence, *Org. Lett.* 12 (2010) 2500–2503.
- T.T. Talele, Natural-products-inspired use of the gem-dimethyl group in medicinal chemistry, *J. Med. Chem.* 61 (2018) 2166–2210.

- [33] K. Kunzelmann, Y. Tian, J.R. Martins, D. Faria, P. Kongsuphol, J. Ousingawatt, F. Thevenod, E. Roussa, J. Rock, R. Schreiber, Anoctamins, *Pflügers Arch.* 462 (2011) 195–208.
- [34] F. Huang, J.R. Rock, B.D. Harfe, T. Cheng, X. Huang, Y.N. Jan, L.Y. Jan, Studies on expression and function of the TMEM16A calcium-activated chloride channel, *Proc. Natl. Acad. Sci. U. S. A.* 106 (2009) 21413–21418.
- [35] M.R. Opp, P.L. Rady, T.K. Hughes Jr., P. Cadet, S.K. Tyring, E.M. Smith, Human immunodeficiency virus envelope glycoprotein 120 alters sleep and induces cytokine mRNA expression in rats, *Am. J. Physiol.* 270 (1996) 963–970.
- [36] C.R. Bader, D. Bertrand, R. Schlichter, Calcium-activated chloride current in cultured sensory and parasympathetic quail neurons, *J. Physiol.* 394 (1987) 125–148.
- [37] Y. Sui, M. Sun, F. Wu, L. Yang, W. Di, G. Zhang, L. Zhong, Z. Ma, J. Zheng, X. Fang, T. Ma, Inhibition of TMEM16A expression suppresses growth and invasion in human colorectal cancer cells, *PLoS ONE* 9 (2014) e115443.
- [38] Y. Li, J. Zhang, S. Hong, ANO1 as a marker of oral squamous cell carcinoma and silencing ANO1 suppresses migration of human SCC-25 cells, *Med. Oral Patol. Oral Cir. Bucal.* 19 (2014) e313–319.
- [39] A. Britschgi, A. Bill, H. Brinkhaus, C. Rothwell, I. Clay, S. Duss, et al., Calcium-activated chloride channel ANO1 promotes breast cancer progression by activating EGFR and CAMK signaling, *Proc. Natl. Acad. Sci. U. S. A.* 110 (2013) E1026–1034.
- [40] W. Liu, M. Lu, B. Liu, Y. Huang, K. Wang, Inhibition of Ca^{2+} -activated Cl^- channel ANO1/TMEM16A expression suppresses tumor growth and invasiveness in human prostate carcinoma, *Cancer Lett.* 326 (2012) 41–51.
- [41] U. Duvvuri, D.J. Shiwardski, D. Xiao, C. Bertrand, X. Huang, R.S. Edinger, J.R. Rock, H.D. Harfe, B.J. Henson, K. Kunzelmann, R. Schreiber, R.S. Seethala, A.M. Eglhoff, X. Chem, V.W. Lui, J.R. Grandis, S.M. Gollin, TMEM16A induces MAPK and contributes directly to tumorigenesis and cancer progression, *Cancer Res.* 72 (2012) 3270–3281.
- [42] A. Picollo, M. Malvezzi, A. Accardi, TMEM16 proteins: unknown structure and confusing functions, *J. Mol. Biol.* 427 (2015) 94–105.
- [43] Y. Zhang, Z. Zhang, S. Xiao, J. Tien, S. Le, T. Le, L.Y. Jan, H. Yang, Inferior olivary TMEM16B mediates cerebellar motor learning, *Neuron* 95 (2017) 1103–1111.
- [44] F. Neureither, K. Ziegler, C. Pitzer, S. Frings, F. Mohrlen, Impaired motor coordination and learning in mice lacking anoctamin 2 calcium-gated chloride channels, *Cerebellum* 16 (2017) 929–937.
- [45] Y. Seo, K. Ryu, J. Park, D.K. Jeon, S. Jo, H.K. Lee, W. Namkung, Inhibition of ANO1 by luteolin and its cytotoxicity in human prostate cancer PC-3 cells, *PLoS ONE* 12 (2017) e0174935.
- [46] Y. Seo, H.K. Lee, J. Park, D.K. Jeon, S. Jo, M. Jo, W. Namkung, Ani9, A novel potent small-molecule ANO1 inhibitor with negligible effect on ANO2, *PLoS ONE* 11 (2016) e0155771.
- [47] A. Bill, A. Gutierrez, S. Kulkarni, C. Kemp, D. Bonenfant, H. Voshol, U. Duvvuri, L.A. Gaither, ANO1/TMEM16A interacts with EGFR and correlates with sensitivity to EGFR-targeting therapy in head and neck cancer, *Oncotarget* 6 (2015) 9173–9188.
- [48] H. Wang, L. Zou, K. Ma, J. Yu, H. Wu, M. Wei, Q. Xiao, Cell-specific mechanisms of TMEM16A Ca^{2+} -activated chloride channel in cancer, *Mol. Cancer* 16 (2017) 152.
- [49] Y. Seo, J. Kim, J. Chang, S.S. Kim, W. Namkung, I. Kim, Synthesis and biological evaluation of novel Ani9 derivatives as potent and selective ANO1 inhibitors, *Eur. J. Med. Chem.* 160 (2018) 245–255.
- [50] Y. Seo, J. Park, M. Kim, H.K. Lee, J.H. Kim, J.H. Jeong, W. Namkung, Inhibition of ANO1/TMEM16A chloride channel by idebenone and its cytotoxicity to cancer cell lines, *PLoS ONE* 10 (2015) e0133656.
- [51] W. Namkung, P.W. Phuan, A.S. Verkman, TMEM16A inhibitors reveal TMEM16A as a minor component of calcium-activated chloride channel conductance in airway and intestinal epithelial cells, *J. Biol. Chem.* 286 (2011) 2365–2374.
- [52] W. Namkung, J.R. Thiagarajah, P.W. Phuan, A.S. Verkman, Inhibition of Ca^{2+} -activated Cl^- channels by gallotannins as a possible molecular basis for health benefits of red wine and green tea, *FASEB J.* 24 (2010) 4178–4186.
- [53] M. Nayak, I. Kim, Alkyne carbonyl metathesis as a means to make 4-acyl chromenes: syntheses of (\pm)-deguelin and (\pm)-munduserone, *J. Org. Chem.* 80 (2015) 11460–11467.
- [54] G.E. Henry, H. Jacobs, A short synthesis of 5-methoxy-2,2-dimethyl-2H-1-benzopyran-6-propanoic acid methyl ester, *Tetrahedron* 57 (2001) 5335–5338.
- [55] P.T. Phan, T.T. Nguyen, H.T. Nguyen, B.N. Le, T.T. Vu, D.C. Tran, T.N. Pham, Synthesis and bioactivity evaluation of novel 2-salicyloylbenzofurans as anti-bacterial agents, *Molecules* 22 (2017) 687.
- [56] Y.H. Seo, K. Damodar, J.K. Kim, J.G. Jun, Synthesis and biological evaluation of 2-arylbenzofurans, rugchalcones A, B and their derivatives as potent anti-inflammatory agents, *Bioorg. Med. Chem. Lett.* 26 (2016) 1521–1524.
- [57] H. Gao, X. Zhang, X.J. Pu, X. Zheng, B. Liu, G.X. Rao, C.P. Wan, Z.W. Mao, 2-Benzoylbenzofuran derivatives possessing piperazine linker as anticancer agents, *Bioorg. Med. Chem. Lett.* 29 (2019) 806–810.
- [58] S. Boddupally, P. Jyothi, M.V.B. Rao, K.P. Rao, Design and synthesis of anti-microbial active (*E*)-(3-(substituted-styryl)-7H-furo[2,3-*f*]chromen-2-yl)(phenyl)methanone derivatives and their in silico molecular docking studies, *J. Heterocycl. Chem.* 56 (2019) 73–80.
- [59] P. Kushwaha, A.K. Tripathi, S. Gupta, P. Kothari, A. Upadhyay, N. Ahmad, T. Sharma, M. Siddigi, R. Trivedi, K.V. Sashidhara, Synthesis and study of benzofuran-pyran analogs as BMP-2 targeted osteogenic agents, *Eur. J. Med. Chem.* 156 (2018) 103–117.
- [60] C. Zhuang, W. Zhang, C. Sheng, W. Zhang, C. Xing, Z. Miao, Chalcone: A privileged structure in medicinal chemistry, *Chem. Rev.* 117 (2017) 7762–7810.
- [61] P. Wu, M. Givskov, T.E. Nielsen, Reactivity and synthetic applications of multi-component Pétasis reactions, *Chem. Rev.* 11245–11290 (2019).
- [62] N.R. Candeias, F. Montalbano, P.M. Cal, P.M. Gois, Boronic acids and esters in the Pétasis-borono Mannich multicomponent reaction, *Chem. Rev.* 110 (2010) 6169–6193.
- [63] N.A. Pétasis, I. Akritopoulou, The boronic acid mannich reaction: a new method for the synthesis of geometrically pure allylamines, *Tetrahedron Lett.* 34 (1993) 583–586.
- [64] V. Pandey, B. Wang, C.D. Mohan, A.R. Raquib, S. Rangappa, V. Srinivasa, J.E. Fuchs, K.S. Girish, T. Zhu, A. Bender, L. Ma, Z. Yin, Basappa, K.S. Rangappa, P.E. Lobie, Discovery of a small-molecule inhibitor of specific serine residue BAD phosphorylation, *Proc. Natl. Acad. Sci. U. S. A.* 115 (2018) E10505–10514.
- [65] P. Doan, A. Karjalainen, J.G. Chandraseelan, O. Sandberg, O. Yli-Harja, T. Rosholm, R. Franzen, N.R. Candeias, M. Kandhavelu, Synthesis and biological screening for cytotoxic activity of *N*-substituted indolines and morpholines, *Eur. J. Med. Chem.* 120 (2016) 296–303.
- [66] Y. Xu, N.Y. Wang, X.J. Song, Q. Lei, T.H. Ye, X.Y. You, W.Q. Zuo, Y. Xia, L.D. Zhang, L.T. Yu, Discovery of novel *N*-(5-(tert-butyl)isoxazol-3-yl)-*N'*-phenylurea analogs as potent FLT3 inhibitors and evaluation of their activity against acute myeloid leukemia in vitro and in vivo, *Bioorg. Med. Chem.* 23 (2015) 4333–4343.
- [67] X.D. Yang, W.C. Wan, X.Y. Deng, Y. Li, L.J. Yang, L. Li, H.B. Zhang, Design, synthesis and cytotoxic activities of novel hybrid compounds between 2-phenylbenzofuran and imidazole, *Bioorg. Med. Chem. Lett.* 22 (2012) 2726–2729.
- [68] F. Baharloo, M.H. Moslemian, H. Nadri, A. Asadipour, M. Mahdavi, S. Emami, L. Firoozpour, R. Mohebat, A. Shafiee, A. Foroumadi, Benzofuran-derived benzylpyridinium bromides as potent acetylcholinesterase inhibitors, *Eur. J. Med. Chem.* 93 (2015) 196–201.
- [69] S.B. Pattle, N. Utjesanovic, A. Togo, L. Wells, B. Conn, H. Monaghan, E. Junor, I. Johannessen, K. Cuschieri, S. Talbot, Copy number gain of 11q13.3 genes associates with pathological stage in hypopharyngeal squamous cell carcinoma, *Genes Chromosomes Cancer* 56 (2017) 185–198.
- [70] C. Ruiz, J.R. Martins, F. Rudin, S. Schneider, T. Dietsche, C.A. Fischer, L. Tornillo, L.M. Terracciano, R. Schreiber, L. Bubendorf, K. Kunzelmann, Enhanced expression of ANO1 in head and neck squamous cell carcinoma causes cell migration and correlates with poor prognosis, *PLoS ONE* 7 (2012) e43265.
- [71] Y. Song, J. Gao, L. Guan, X. Chen, J. Gao, K. Wang, Inhibition of ANO1/TMEM16A induces apoptosis in human prostate carcinoma cells by activating TNF- α signaling, *Cell Death Dis.* 9 (2018) 703.
- [72] S. Dang, S. Feng, J. Tien, C.J. Peters, D. Bulkley, M. Lolicato, J. Zhao, K. Zuberbühler, W. Ye, L. Qi, T. Chen, C.S. Craik, Y.N. Jan, D.L. Minor Jr, Y. Cheng, L.Y. Jan, Cryo-EM structures of the TMEM16A calcium-activated chloride channel, *Nature* 552 (2017) 426–429.
- [73] Y.H. Lee, Yi, GS, Prediction of Novel Anoctamin1 (ANO1) Inhibitors Using 3D-QSAR Pharmacophore Modeling and Molecular Docking, *Int. J. Mol. Sci.* 19 (2018) 3204.
- [74] L.G. Ferreira, R.N. Dos Santos, G. Oliva, A.D. Andricopulo, Molecular docking and structure-based drug design strategies, *Molecules.* 20 (7) (2015) 13384–13421.